Mon. Not. R. Astron. Soc. **383,** 755–776 (2008) doi:10.1111/j.1365-2966.2007.12587.x

The detectability of baryonic acoustic oscillations in future galaxy surveys

R. E. Angulo,★ C. M. Baugh,★ C. S. Frenk★ and C. G. Lacey★
Institute for Computational Cosmology, Department of Physics, University of Durham, South Road, Durham DH1 3LE

Accepted 2007 October 12. Received 2007 October 12; in original form 2007 February 20

ABSTRACT

We assess the detectability of baryonic acoustic oscillation (BAO) in the power spectrum of galaxies using ultralarge volume *N*-body simulations of the hierarchical clustering of dark matter and semi-analytical modelling of galaxy formation. A step-by-step illustration is given of the various effects (non-linear fluctuation growth, peculiar motions, non-linear and scale-dependent bias) which systematically change the form of the galaxy power spectrum on large scales from the simple prediction of linear perturbation theory. Using a new method to extract the scale of the oscillations, we nevertheless find that the BAO approach gives an unbiased estimate of the sound horizon scale. Sampling variance remains the dominant source of error despite the huge volume of our simulation box ($=2.41\,h^{-3}\,\mathrm{Gpc}^3$). We use our results to forecast the accuracy with which forthcoming surveys will be able to measure the sound horizon scale, s, and, hence constrain the dark energy equation of state parameter, w (with simplifying assumptions and without marginalizing over the other cosmological parameters). Pan-STARRS could potentially yield a measurement with an accuracy of $\Delta s/s = 0.5$–0.7 per cent (corresponding to $\Delta w \approx 2$–3 per cent), which is competitive with the proposed WFMOS survey ($\Delta s/s = 1$ per cent $\Delta w \approx 4$ per cent). Achieving $\Delta w \leqslant 1$ per cent using BAO alone is beyond any currently commissioned project and will require an all-sky spectroscopic survey, such as would be undertaken by the SPACE mission concept under proposal to ESA.

Key words: methods: *N*-body simulations – cosmology: theory – large-scale structure of Universe.

1 INTRODUCTION

The discovery that the rate of expansion of the Universe is apparently accelerating was one of the key advances in physical cosmology in the 1990s (Riess et al. 1998; Perlmutter et al. 1999). Understanding the nature of the dynamically dominant dark energy, which is believed to be responsible for this behaviour, is one of the biggest challenges now facing cosmologists.

Over the past decade our knowledge of the basic cosmological parameters, which describe the content of the Universe, its expansion history and ultimate fate has improved tremendously. This progress is the result of advances on two fronts: the advent of data sets which have provided fresh views of the Universe with unprecedented detail and the development of the theoretical machinery required to interpret these new measurements. Currently, the values of many cosmological parameters are known to an accuracy of around 10 per cent (albeit with caveats regarding degeneracies between certain combinations of parameters and also regarding the precise number of parameters that are allowed to vary in the cosmological model; see e.g. Sánchez et al. 2006).

★E-mail: raul.angulo@durham.ac.uk (REA); c.m.baugh@durham.ac.uk (MB); c.s.frenk@durham.ac.uk (CSF); cedric.lacey@durham.ac.uk (CL)

The cold dark matter (CDM) model has emerged as the most plausible description of our Universe. In the most successful version of this model, more than 70 per cent of the density required to close the Universe is in the form of dark energy. Currently, there is no model which can reconcile the magnitude of the dark energy component with the value expected from particle physics arguments. A simple phenomenological description of the dark energy is provided by the equation of state that relates its pressure, P, and density, ρ, which is encapsulated in the parameter $w = P/\rho\,c^2$. If the dark energy has the form of the cosmological constant, $w = -1$. The indications are that the dark energy now has a form close to that expected for a cosmological constant (Riess et al. 2004; Sánchez et al. 2006). However, in the absence of a theoretical model for the dark energy, it is possible that the equation of state could depend on space and/or time.

A whole range of experiments and surveys is being planned which number amongst their goals determining the equation of state of the dark energy as a function of redshift (for a discussion, see Albrecht et al. 2006; Peacock & Schneider 2006). Several techniques are being considered, which are sensitive to the influence of the dark energy on various features of the cosmological world model. These include the Hubble diagram of Type Ia supernovae (SNe Ia), counts of clusters of galaxies, the weak gravitational lensing pattern of faint galaxies and the measurement of the baryonic acoustic oscillation

(BAO) scale in the matter distribution as a function of redshift. The measurements and data analysis required to obtain useful constraints on the equation of state parameter are so demanding, and so open to potential systematic errors, that it is necessary to pursue as many different avenues as possible.

In this paper, we focus on the test using the BAO. The BAO is the name given to a series of peaks and troughs on scales on the order of $100\,h^{-1}$ Mpc, imprinted on the power spectrum of matter fluctuations prior to the epoch of last scattering, when the matter and radiation components of the Universe were coupled (Peebles & Yu 1970). The BAO are the counterpart of the acoustic peaks seen in the power spectrum of the temperature of the cosmic microwave background (CMB) radiation, though they have a different phase and a much smaller amplitude (Sunyaev & Zeldovich 1970; Press & Vishniac 1980; Hu & Sugiyama 1996; Eisenstein & Hu 1998; Meiksin, White & Peacock 1999). The wavelength of the BAO is related to the size of the sound horizon at recombination. This does not depend on the amount or nature of the dark energy, but on the physical density of matter ($\Omega_{\rm m}h^2$) and baryons ($\Omega_{\rm b}h^2$). Given the values of these parameters, for example, from the CMB or large-scale structure data, the sound horizon scale is known and can be treated as a standard ruler. The *apparent* size of this feature in the power spectrum of galaxies or galaxy clusters does depend on the dark energy and its equation of state through the angular diameter distance–redshift relation (e.g. Blake & Glazebrook 2003; Hu & Haiman 2003)

BAO in the galaxy distribution were first glimpsed in the early stages of the 'two-degree-Field Galaxy Redshift Survey' (2dFGRS) (Percival et al. 2001) and finally detected in the power spectrum of the completed 2dFGRS (Cole et al. 2005). The equivalent feature, a spike, was also found in the correlation function measured from the luminous red galaxy (LRG) sample of the Sloan Digital Sky Survey (SDSS) (Eisenstein et al. 2005). Cole et al. used the BAO to constrain the parameter combination ($\Omega_{\rm M}/\Omega_{\rm b}$, $\Omega_{\rm M}$) (where $\Omega_{\rm M}$ and $\Omega_{\rm b}$ denote the matter and baryon density parameters, respectively). Eisenstein et al. used the location of the spike in the correlation function to constrain the absolute distance to the median redshift of the SDSS LRG sample and hence constrained the value of $\Omega_{\rm M}$. Hütsi (2006a,b) carried out a power-spectrum analysis of a similar LRG sample, and combined this measurement with other data sets to constrain the values of cosmological parameters. More recently, the BAO have been extracted from the power spectrum measured from a much larger sample of SDSS LRGs to constrain $\Omega_{\rm M}$ and $\Omega_{\rm b}/\Omega_{\rm m}$ (Tegmark et al. 2006; Blake et al. 2007; Padmanabhan et al. 2007; Percival et al. 2007). To date, measurements of the BAO have only yielded constraints on the dark energy equation of state when combined with other data sets, such as the spectrum of temperature fluctuations in the microwave background or when restrictive priors have been adopted on certain parameters, such as the Hubble constant.

The bulk of the work in the literature on the usefulness of the BAO has relied upon linear perturbation theory to assess the detectability of the features and to forecast the errors on the recovered value of w (Blake & Glazebrook 2003; Hu & Haiman 2003; Blake & Bridle 2005; Glazebrook & Blake 2005; Blake et al. 2006; Parkinson et al. 2007). There are, however, a range of dynamical and statistical effects which can alter the appearance of the power spectrum relative to the linear theory prediction, even on the scale of the BAO, which we review in this paper (Seo & Eisenstein 2003; Angulo et al. 2005; Seo & Eisenstein 2005; Springel et al. 2005; Eisenstein, Seo & White 2007). Some simulation work has been done to study these effects, mostly using computational cubes of side $500\,h^{-1}$ Mpc (Seo & Eisenstein 2003, 2005; Springel et al. 2005; Eisenstein et al. 2007). These are only a small factor (2–3) bigger than the scale of the fluctuations of interest. Calculations with small boxes are subject to large sampling fluctuations and may even miss some features of the non-linear growth of large-scale fluctuations through the absence of long-wavelength density fluctuations (Crocce & Scoccimarro 2006a). Very recently, larger simulation volumes have been used, of around a cubic gigaparsec and larger (Angulo et al. 2005; Schulz & White 2006; Huff et al. 2007; Koehler, Schuecker & Gebhardt 2007). However, such studies have tended to have relatively poor mass resolution, making it difficult to model galaxies without resorting to simplified biasing prescriptions (e.g. Cole et al. 1998).

Given the significant commitment of resources required by the proposed galaxy surveys and the level of precision demanded by the BAO approach, it is imperative to ensure that accurate theoretical predictions are available both to help in the design of the survey strategy and to extract the maximum amount of information from the observations. This is a tough challenge computationally, because it requires ultralarge volume *N*-body simulations with sufficient mass resolution to identify the haloes likely to host the galaxies to be seen in the surveys, and a realistic model to populate these haloes with galaxies.

In this paper, we use a combination of suitable *N*-body simulations and a semi-analytical model of galaxy formation to assess the visibility of the BAO. In Section 2, we describe the suite of *N*-body simulations used and outline the semi-analytical model. Section 3 gives a blow-by-blow account of how the power spectrum changes relative to the simple prediction of linear perturbation theory, as additional layers of realism are added to the modelling, starting with dark matter and ending with galaxies. We set out our approach for constraining the dark energy equation of state in Section 4, and present our results in Section 5. We give our conclusions in Section 6.

2 METHOD

In this section, we introduce the theoretical tools used to produce synthetic galaxy catalogues. First, we describe the *N*-body simulations (Section 2.1) which consist of a high-resolution run (Section 2.1.1) and an ensemble of lower resolution runs (Section 2.1.2). Next, we discuss the measurement of power spectra from discrete distributions of objects and use the ensemble of low-resolution simulations to estimate the errors on the power-spectrum measurement (Section 2.1.3). In the second part of this section, we explain how a galaxy formation model is used to populate the high-resolution *N*-body simulation with galaxies (Section 2.2).

2.1 *N*-body simulations

The *N*-body method is a long-established computational technique which is used to follow the growth of cosmological structures through gravitational instability (see e.g. the reviews by Bertschinger 1998 and Springel, Frenk & White 2006). Our goal in this paper is to simulate the formation of structure within a sufficiently large volume to follow the growth of fluctuations accurately on the scale of the BAO, and with similar statistics for power-spectrum measurements to those expected in forthcoming surveys. At the same time, we require a mass resolution which is adequate to identify the dark matter haloes likely to host the galaxies which will be seen in these surveys. To achieve these aims, we use a memory-efficient version of the GADGET-2 code of Springel (2005), which was kindly provided to us by Volker Springel and the Virgo Consortium.

We use two types of calculation: a high-resolution simulation, labelled the 'Baryon Acoustic Simulation at the ICC' or BASICC, which is able to track galactic haloes, and an ensemble of lower resolution simulations, labelled L-BASICC, which we use to study the statistics of power-spectrum measurements on large scales. Here, we describe some of the common features of the simulations, before moving on to outline specific details in Sections 2.1.1 and 2.1.2.

We adopt a ΛCDM cosmology with the same parameters used in the Millennium Simulation (Springel et al. 2005), which are broadly consistent with the latest constraints from the CMB data and large-scale structure measurements (Sánchez et al. 2006; Spergel et al. 2007). The values of the parameters are: the matter density parameter, $\Omega_{\rm M} = 0.25$, the energy density parameter for the cosmological constant, $\Omega_\Lambda = 0.75$, the normalization of density fluctuations, $\sigma_8 = 0.9$ and Hubble constant, $h = H_0/(100\,{\rm km\ s^{-1}\,Mpc^{-1}}) = 0.73$.

Due to memory restrictions, the Fourier mesh used to set up the initial particle displacements has a dimension of 1580^3 grid points which is not commensurate with the cube root of the particle number mesh. We therefore avoided using a regular particle grid to set up the initial conditions, as this would have led to a spurious feature in the power spectrum of the initial conditions at the beat frequency between the particle grid and the Fourier mesh. Instead, we used a glass-like distribution (White 1994; Baugh, Gaztanaga & Efstathiou 1995). The input power spectrum of density fluctuations in linear perturbation theory is calculated using the CAMB package of Lewis, Challinor & Lasenby (2000). The amplitude of the Fourier modes is drawn from a Rayliegh distribution with mean equal to the linear theory power spectrum and the phase is drawn at random from the interval 0–2π. The initial density field is generated by perturbing particles from the glass-like distribution, using the approximation of Zel'dovich (1970).

The simulations were started at a redshift of $z = 63$. The Zel'dovich (1970) approximation used to set up the initial pattern of density fluctuations produces transients which can be seen in clustering signal measured for the dark matter at expansion factors close to the starting redshift (Efstathiou et al. 1985; Baugh, Gaztanaga & Efstathiou 1995; Crocce, Pueblas & Scoccimarro 2006). Later on, we will use the power spectrum from a high-redshift output from the simulation, $z = 15$, as a proxy for linear perturbation theory, so it is important to check that this power spectrum in particular, and also the power spectra measured at all subsequent outputs are insensitive to the choice of starting redshift. We test this by comparing the power spectrum of the dark matter at $z = 15$ in our standard run with the spectrum measured in a test run which started at $z = 127$, but which did not run all the way through to $z = 0$. The top panel of Fig. 1 shows that the power spectra measured for the dark matter in these two cases, divided by the power spectrum predicted by linear perturbation theory at $z = 15$. The fluctuations in the measured power at low wavenumbers around the linear theory prediction reflect the sample variance noise which is not negligible even in a simulation of the volume of the BASICC. The lower panel in Fig. 1 shows the $z = 15$ power spectrum measured from the run started at $z = 63$ divided by that measured from the run started at $z = 127$. At large wavenumbers, the effect of transients is visible, although quite small, ∼1 per cent. The focus of this paper, however, is the form of the power spectrum over wavenumbers smaller than $k = 0.4\,h\,{\rm Mpc^{-1}}$, for which the spectra measured at $z = 15$ for the two different choices of starting redshift agree to better than 0.3 per cent. Our results are therefore unaffected by any transients resulting from the use of the Zel'dovich approximation.

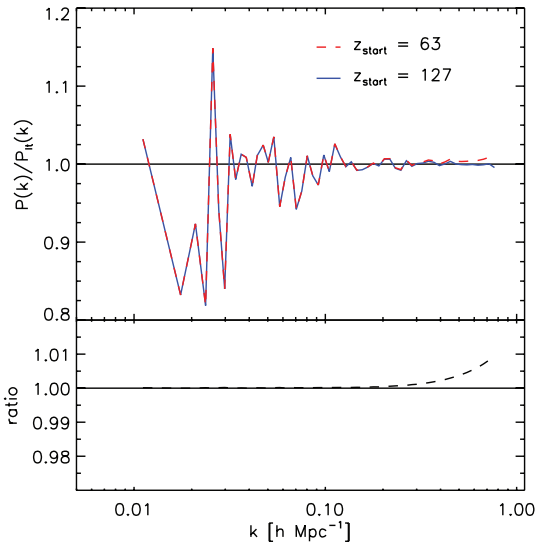

Figure 1. A test of the choice of starting redshift used in the *N*-body simulations. The upper panel compares the power spectrum measured at $z = 15$ in the BASICC when the simulation is started at $z = 63$ (dashed red curve) and at $z = 127$ (solid blue curve). The power spectra plotted in the upper panel have been divided by the linear perturbation theory prediction for the dark matter power spectrum at $z = 15$. The lower panel shows the ratio between the power spectrum measured from the simulation started at redshift 63 to that measured from the run which started at redshift 127.

2.1.1 The high-resolution simulation: the BASICC

The BASICC simulation covers a comoving cubical region of side $1340\,h^{-1}$ Mpc, in which the dark matter is represented by more than 3 billion (1448^3) particles. The equivalent Plummer softening length in the gravitational force is $\epsilon = 50\,h^{-1}$ kpc, giving a dynamic range in length of almost 27 000. The volume of the computational box, $2.41\,h^{-3}\,{\rm Gpc^3}$, is almost 20 times the volume of the Millennium Simulation (Springel et al. 2005), and more than three times the volume of the catalogue of LRGs from the SDSS used to detect the acoustic peak by Eisenstein et al. (2005). The BASICC volume is within a factor of 2 of that proposed for a survey with WFMOS at $z \sim 1$ (Glazebrook et al. 2005). The simulation occupied the full 0.5 TB of RAM of the second upgrade of the Cosmology Machine at Durham. The run took 11 CPU days on 506 processors, the equivalent of 130 000 cpu-hours.

The particle mass in the BASICC simulation is $m_{\rm p} = 5.49 \times 10^{10}\,h^{-1}\,{\rm M_\odot}$. This is approximately 64 times larger than the particle mass used in the Millennium Simulation. The mass resolution limits the usefulness of dark matter halo merger trees from the BASICC, so we have chosen to output at a modest selection of redshifts: $z = 0$, 0.3, 0.5, 1, 2, 3, 4, 6, 8, 10, 15 and 63. Each of these outputs occupies ∼100 GB of disc space. In each snapshot we have identified groups of dark matter particles using a friends-of-friends algorithm (Davis et al. 1985) with a linking length of 0.2 times the mean interparticle separation. We have stored groups with 10 or more particles, i.e. haloes more massive than $5.49 \times 10^{11}\,h^{-1}\,{\rm M_\odot}$. There are 17 258 579 haloes in the $z = 0$ output of the simulation with 10 or more particles. The most massive halo has a mass of $6.74 \times 10^{15}\,h^{-1}\,{\rm M_\odot}$ and 860 haloes have a mass in excess of the Coma cluster ($\approx 10^{15}\,h^{-1}\,{\rm M_\odot}$).

The BASICC simulation sits between the Millennium and Hubble Volume (Evrard et al. 2002) Simulations. Its unique combination of

Table 1. The values of some of the basic parameters used in the simulations. The columns are as follows. (1) The name of the simulation. (2) The number of particles. (3) The mass of a dark matter particle. (4) The softening parameter used in the gravitational force. In both cases, the length of the computational box is $1340\,h^{-1}$ Mpc, and the same cosmological parameters are used, as given in Section 2.1.

	$N_{\rm p}$	$m_{\rm dm}$ ($h^{-1}\,{\rm M}_{\odot}$)	ϵ (h^{-1} kpc)
BASICC	3.03×10^9	5.49×10^{10}	50
L-BASICC	8.99×10^7	1.85×10^{12}	200

mass resolution and volume makes it ideal for studying the large-scale distribution of galaxies and clusters alike.

2.1.2 *The ensemble of low-resolution simulations: L-BASICC*

We also generated an ensemble of 50 'low-resolution' simulations to study the sample variance in the BASICC and to test an analytic model for the errors expected on measurements of the power spectrum, which we discuss in the next subsection. These low-resolution runs (L-BASICC) have exactly the same cosmological parameters as the BASICC and the same box size (see Table 1), but they have fewer particles (448^3). For each realization, a different random seed is used to set up the initial density field. The starting redshift of these simulations is $z = 63$. The particle mass is comparable to that employed in the Hubble Volume Simulation (Evrard et al. 2002). Each L-BASICC simulation took 0.8 d to run on 16 processors of the third upgrade of the Cosmology Machine. The total volume of the ensemble is $120\,h^{-3}$ Gpc^3, more than four times that of the Hubble Volume, making this a unique resource for studying the frequency of rare objects in a ΛCDM universe. For L-BASICC, the position and velocity are stored for every particle at four output times ($z = 0.0$, 0.5, 0.9, 3.8); we also produce a halo catalogue at each redshift retaining objects with 10 or more particles (corresponding to a mass of $1.8 \times 10^{13}\,h^{-1}\,{\rm M}_{\odot}$). As we shall see in later sections, the ensemble allows us to assess whether or not a particular result is robust or simply due to sampling fluctuations. Due to their limited mass resolution, it is not feasible to populate these simulations with galaxies using the method outlined below (Section 2.2).

2.1.3 *Power-spectrum estimation and errors*

The two-point statistics of clustering, the correlation function, and its Fourier transform, the power spectrum, $P(k)$, are the most commonly employed measurements of clustering. In this paper we focus on the power spectrum; in Sanchez et al. (in preparation), we address the visibility of the acoustic oscillations in the correlation function. The standard way to quantify the amplitude of a density fluctuation is by means of the density contrast, $\delta(x,t) = (\rho(x,t) - \bar{\rho})/\bar{\rho}$. If we consider the Fourier transform of the density contrast, $\rho_{\rm k}$, then the power spectrum is defined as the modulus squared of the mode amplitude, $P(k) = \langle |\,\delta_{\rm k}|^2 \rangle$.

There are two steps in the computation of the power spectrum from a distribution of discrete objects, such as dark matter particles, dark haloes or galaxies. First, a density field is constructed by assigning the objects to mesh points on a cubic grid. In the simplest mass assignment scheme, the nearest grid point, the contribution of each object to the density field is confined to the cell in which it is located. In higher order assignment schemes, the mass of the particle is shared with adjacent cells. Here, we use the cloud-in-cell assignment scheme (see Hockney & Eastwood 1981). Secondly, we perform a fast Fourier transform of the density field. The power spectrum is obtained by spherically averaging the resulting Fourier mode amplitudes in annuli of radius $\delta k = 2\,\pi/L = 0.0047\,h\,{\rm Mpc}^{-1}$.

The mesh we use to store the density field has $N_{\rm FFT}^3 = 512^3$ grid points. Estimating the density on a grid alters the form of the power spectrum at wavenumbers approaching the Nyquist frequency of the grid ($k_{\rm Nyquist} = 2\pi/L\,N_{\rm FFT}/2 = 1.2\,h\,{\rm Mpc}^{-1}$ in our case). The degree of modification and the precise wavenumber above which the power spectrum is distorted depend upon the choice of assignment scheme (Hatton 1999; Jing 2005). In practice, for the size of FFT mesh we use, this has little impact on the recovered power spectrum for wavenumbers of interest; the measured amplitude differs by less than 1 per cent from the true value at a wavenumber $k \sim 0.8\,h\,{\rm Mpc}^{-1}$; in most cases we focus on the form of the power spectrum on large scales, $k < 0.4\,h\,{\rm Mpc}^{-1}$. Nevertheless, we correct for the effects of the cloud-in-cell assignment scheme by dividing each mode by the Fourier transform of a cubical top-hat:

$$\delta(k_x, k_y, kz) \Rightarrow \frac{\delta(k_x, k_y, kz)}{{\rm sinc}\left(\frac{k_x L}{2N_{\rm FFT}}\right)\,{\rm sinc}\left(\frac{k_y L}{2N_{\rm FFT}}\right)\,{\rm sinc}\left(\frac{k_z L}{2N_{\rm FFT}}\right)}, \quad (1)$$

where

$${\rm sinc}(x) = \frac{\sin(x)}{x}. \quad (2)$$

Note this is different from the approach taken by Jing (2005), who applied a correction to the spherically averaged power spectrum.

A further possible distortion to the form of the measured power spectrum is discreteness noise and the associated Poisson or shot noise. Poisson-sampling a continuous-density field with point objects of space density, $\bar{n}$, introduces a spurious contribution that should be subtracted from the measured power spectrum: $P_{\rm corr}(k) = P_{\rm meas}(k) - 1/\bar{n}$. In the case of dark matter halo centres or galaxies, the need for such a correction is justified. However, in the case of dark matter particles in our simulations, one should *not* subtract Poisson shot noise from the power spectrum because the particles were initially laid down by perturbing a glass-like configuration which is sub-Poissonian in nature. This is clear from Fig. 2, which shows the power spectrum measured for the dark matter in the initial conditions of the BASICC. The red curve shows the spectrum measured in the simulation and the smooth green curve shows the input spectrum predicted by linear perturbation theory. The two agree remarkably well over a wide range of wavenumbers. The power spectrum of the *unperturbed* glass-like particle distribution is shown by the blue curve. For the wavenumbers of interest, the power spectrum of the glass is many orders of magnitude below the discreteness noise expected for a Poisson distribution of objects with the same space density as the dark matter particles, as shown by the dashed line. In this paper, we do not apply any shot noise correction to power spectra measured for the dark matter, but we do make such a correction for spectra estimated for samples of haloes and galaxies.

To close this subsection, we turn our attention to the error on the measurement of the power spectrum. A commonly used expression for the fractional error in the measured power spectrum was derived by Feldman, Kaiser & Peacok (1994) (see also Efstathiou 1988, for a similar argument applied to the two-point correlation function):

$$\frac{\sigma}{P} = \sqrt{\frac{2}{n_{\rm modes}}}\left(1 + \frac{1}{P\bar{n}}\right), \quad (3)$$

where $n_{\rm modes}$ is the number of Fourier modes present in a spherical shell of width δk, which depends upon the survey volume V: for $k \gg 2\pi/V^{1/3}$, this is given by $n_{\rm modes} = V\,4\pi k^2 \delta k/(2\pi)^3$. The first

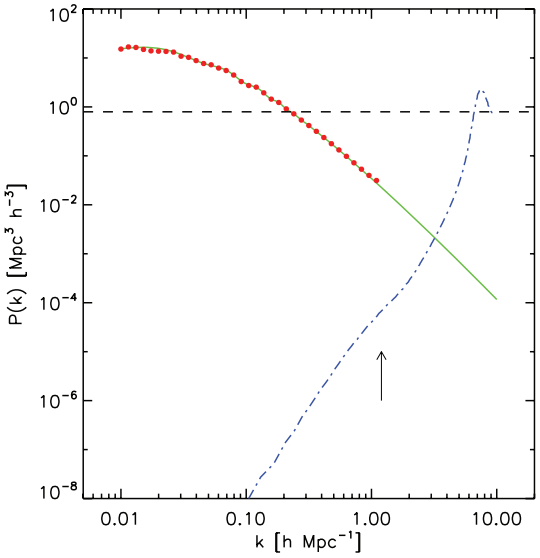

Figure 2. The power spectrum of the dark matter in real space measured at the starting redshift of the BASICC, $z = 63$ (red points). The corresponding prediction of linear perturbation theory is shown by the green (solid) line. The blue (dot–dashed) curve shows the power spectrum of the *unperturbed* glass-like distribution of particle positions. The dashed line shows the Poisson noise expected for the number density of dark matter particles used in the BASICC. The noise of the initial particle distribution is much less than Poisson. The arrow marks the position of the Nyquist frequency of the FFT grid.

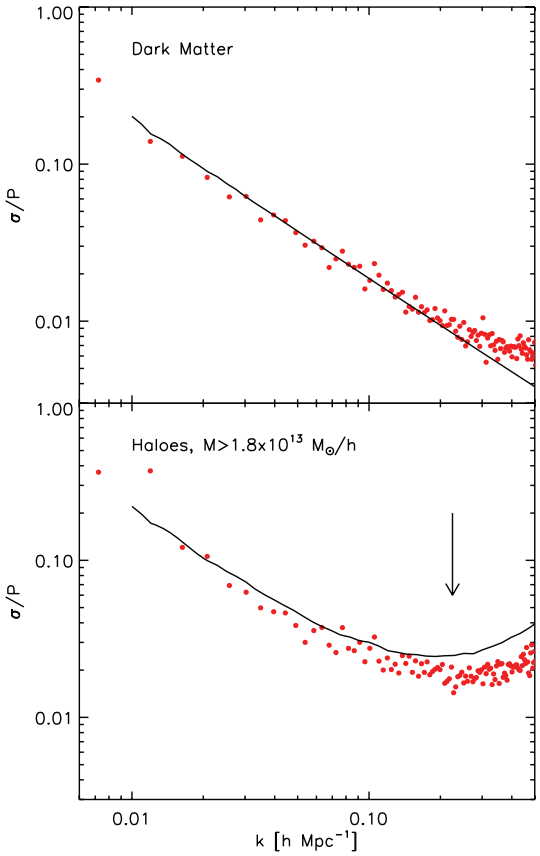

Figure 3. The fractional error in the power spectrum of the dark matter (top panel) and in the power spectrum of haloes more massive than $1.8 \times 10^{13}\,h^{-1}\,\mathrm{M}_\odot$ (bottom panel), estimated using the low-resolution simulations from the dispersion of $P(k)$ around the ensemble mean. The smooth black curves show the error predicted by the analytical expression given in equation (3). The red points show the scatter from the ensemble of low-resolution simulations. The arrow in the bottom panel shows the wavenumber for which $\bar{n}P(k = 0.2\,h\,\mathrm{Mpc}^{-1}) = 1$.

term on the right-hand side of equation (3) quantifies the sample variance in the measurement, which decreases as the square root of the number of modes or, equivalently, as the square root of the volume probed. The second term arises from the discreteness of the objects under consideration. The combination $P\bar{n}$ quantifies the amplitude of the power spectrum in units of the Poisson shot noise, effectively giving the contrast of the power-spectrum signal relative to the shot noise level. In the case where $P\bar{n} \gg 1$, $\sigma/P \propto 1/k$. On the other hand, when the amplitude of the power spectrum is comparable to the shot noise, and if $P(k) \propto k^{-1}$, then the fractional error in the power is approximately independent of wavenumber. We have tested this prescription in both regimes against the diagonal element of the covariance between power-spectrum measurements extracted from the ensemble of low-resolution simulations, as shown in Fig. 3. Over the wavenumber range of interest, the agreement is reasonably good for samples in which the shot noise is negligible compared to the clustering signal. For samples with low-contrast power measurements, such as is the case for dark matter haloes used in the bottom panel of Fig. 3, the analytic expression works well until $k \sim 0.1\,h\,\mathrm{Mpc}^{-1}$ and then overpredicts the errors by up to 50 per cent. We note that non-linearities and the impact of the window function of a realistic survey could introduce off-diagonal terms in the power-spectrum covariance matrix. In Section 5.3, we compare the constraints on the recovered oscillation scale using the scatter from the ensemble and using the simple mode-counting argument outlined above. We find good agreement which suggests that mode-coupling does not make a significant contribution to the errors on the scales relevant to the BAO.

2.2 Modelling the formation and evolution of galaxies

The *N*-body simulations described in the previous section follow the growth of fluctuations in the mass which is dominated by collisionless matter. To connect the predictions of the CDM theory to forthcoming galaxy surveys, we need to predict which structures host galaxies and how galaxy properties depend on halo mass.

Some authors have chosen to incorporate galaxies into an *N*-body simulation empirically by using a parametric model called a halo occupation distribution function (HOD) to describe the probability distribution of galaxies expected in haloes of a given mass (Benson et al. 2000). The form of the HOD is constrained to reproduce a particular clustering measurement, such as the galaxy correlation function (e.g. Peacock & Smith 2000; Seljak 2000; Scoccimarro et al. 2001; Cooray & Sheth 2002). This approach has been applied to the study of the detectability of acoustic oscillations by several authors (Seo & Eisenstein 2005; Schulz & White 2006; Huff et al. 2007). Two assumptions are made when using the HOD to populate an *N*-body simulation with galaxies. First, the parameterization used for the HOD is assumed to provide an accurate description of the manner in which galaxies populate haloes across a wide range of halo mass. Detailed comparisons between the clustering predictions made using HODs and those obtained directly from simulations of galaxy formation show that in practice, the HODs do a reasonable job (Berlind et al. 2003; Zheng et al. 2005). Recently, one of the fundamental assumptions which underpins the HOD approach has been called into question. Using the Millennium Simulations, Gao,

Springel & White (2005) demonstrated that the clustering of dark matter haloes depends on a second parameter, such as the formation time of the halo, in addition to halo mass (see also Harker et al. 2006 and Wechsler et al. 2006; Wetzel et al. 2007). In practice, for typical galaxy samples, this effect is largely washed out due to the mix of halo properties sampled (Croton, Gao & White 2007). The second implicit assumption in the HOD method when applied to an *N*-body simulation is that all of the haloes in which galaxies are expected to be found can be resolved in the simulation; if the mass resolution of the simulation turns out to be inadequate, then the HOD realized will be distorted to compensate, compared with the true, underlying HOD in the Universe.

In this paper, we take a more physical approach and make an *ab initio* prediction of which dark matter haloes should contain galaxies by modelling the physics of the baryonic component of the Universe. We do this using a semi-analytic model of galaxy formation (for a review of this technique see Baugh 2006). The semi-analytic model describes the key physical processes which are thought to determine the formation and evolution of galaxies. We use the GALFORM code introduced by Cole et al. (2000) and developed in a series of papers (Benson et al. 2002, 2003; Baugh et al. 2005; Bower et al. 2006). The specific model we use is the one proposed by Baugh et al. (2005), which reproduces the abundance of Lyman-break galaxies at $z = 3$ and 4, the number counts of submillimetre detected galaxies (with a median redshift $z \sim 2$), and a rough match to the abundance of LRGs (Almeida et al. 2007b), whilst at the same time giving a reasonable match to the observed properties of local galaxies (e.g. Nagashima et al. 2005a,b; Almeida, Baugh & Lacey 2007a).

A key advantage of using a semi-analytic model is that we can investigate how the manner in which galaxies are selected affects the accuracy with which the acoustic oscillations can be measured. The model predicts the star formation history of each galaxy and uses this to compute a spectrum, broad-band magnitudes and emission-line strengths (for examples of the latter, see Le Delliou et al. 2005, 2006). We can therefore select samples of model galaxies by applying precisely the same criteria which will be applied in the proposed surveys.

Our methodology mirrors the hybrid schemes introduced by Kauffmann, Nusser & Steinmetz (1997) and Benson et al. (2000). We use a Monte Carlo technique to generate merger trees for dark mater haloes since our simulation outputs do not have the resolution in time or mass necessary to allow the construction of merger trees. (See Baugh 2006 for a discussion of the relative merits of these two approaches.)

We first construct a grid of halo masses at the redshift of interest, which extends to lower mass haloes than can be resolved in the simulation. We then generate a number of Monte Carlo realizations of mass assembly histories for each mass on the grid, using the algorithm introduced by Cole et al. (2000). The number of realizations is chosen to allow robust predictions to be made for observables such as the galaxy luminosity function. The halo merger history is input into the semi-analytic code and the properties of the galaxy population are output at the redshift for which the galaxy catalogue is to be constructed. In the calculations in this paper, we output the broad-band magnitudes in the R, I and K bands and the equivalent widths of H_α and O II[3727] for each galaxy. Finally, haloes from the grid are matched with haloes of similar mass identified in the *N*-body simulation. The central galaxy in each halo is assigned to the centre of mass of the matched halo in the simulation. The satellite galaxies are assigned randomly to dark matter particles in the halo. Galaxies placed in the simulation box in this way are called 'resolved galaxies'. The Monte Carlo merger trees will not, of course, correspond in detail with those of the matched haloes in the *N*-body simulation. However, to the extent that the halo assembly bias discussed by Gao et al. (2005) can be neglected, the properties of the trees are statistically similar for haloes in the same mass range.

Because of the finite mass resolution of the *N*-body simulation, galaxy samples generated by populating resolved haloes will be incomplete fainter than some magnitude limit. In principle, since we are using Monte Carlo merger trees, we can follow galaxies down to arbitrarily faint magnitudes *within* a resolved dark matter halo. However, as we consider progressively fainter objects, some fraction of these galaxies should also appear in haloes which the simulation cannot resolve, causing the sample to become incomplete. Thus, in some instances we need to consider galaxies which we would expect to find in haloes below the mass resolution of the simulation. These galaxies are called 'unresolved galaxies' and are placed in the box in the following way. A volume-limited sample of galaxies is generated using the semi-analytic model, with a volume equal to that of the simulation cube. Only galaxies which reside in haloes from the grid which are less massive than the resolution limit of the *N*-body simulation are considered. (Recall that the grid of halo masses used in the semi-analytic calculation extends to lower mass than those resolved in the simulation.) These galaxies are assigned to randomly selected dark matter particles which have *not* been identified as members of haloes identified by the friends-of-friends algorithm. This approach was adopted for one of the mock catalogues used in Cole et al. (2005). As we will see below, the unresolved galaxies are a minority within any of the samples we consider. They have little effect on the measured power spectrum, producing only a modest change in the amplitude of the clustering signal.

We can use the semi-analytic calculation carried out on the grid of halo masses to find the completeness limit of the galaxy catalogue in the *N*-body simulation. To do this, we use the galaxy formation calculation carried out using the grid of halo masses to compute the cumulative luminosity function of galaxies, starting with the brightest galaxy, for two cases: (1) without any restriction on the mass of the halo which hosts the galaxy and (2) considering only those galaxies which reside in haloes above the resolution limit of the simulation. We then divide the second estimate of the cumulative luminosity function by the estimate made without any restriction on halo mass.

The completeness ratios calculated in this way are shown for $z = 0$, 1 and 2 in Fig. 4. The vertical lines show the magnitude limit down to which the 'resolved galaxy' catalogues are 100 per cent complete. The lower panel shows the cumulative luminosity function in the model at the same redshifts, with horizontal lines marking the space density of galaxies at the sample completeness limit. (The magnitudes plotted are observer-frame absolute magnitudes in the R band. The apparent magnitude is obtained by adding the appropriate distance modulus for each redshift. All magnitudes are on the AB scale.) The $z = 2$ sample is complete down to $M_R - 5 \log h = -23$, or, equivalently to a space density of $3.2 \times 10^{-5}\, h^3\, \mathrm{Mpc}^{-3}$. Faintwards of this magnitude, the completeness drops sharply to around 30–40 per cent. The situation is much more encouraging at $z = 1$. Here, the galaxy catalogue is complete to $M_R - 5 \log h = -22.3$ (corresponding to a space density of just under $10^{-4}\, h^3\, \mathrm{Mpc}^{-3}$) and faintwards of this there is a much more modest drop in the fraction of galaxies resolved in the simulation. The simulation resolves around two-thirds of the space density of galaxies expected in the proposed WFMOS survey. At $z = 0$, the galaxy samples are complete to a much higher space density, in excess of $10^{-3}\, h^3\, \mathrm{Mpc}^{-3}$.

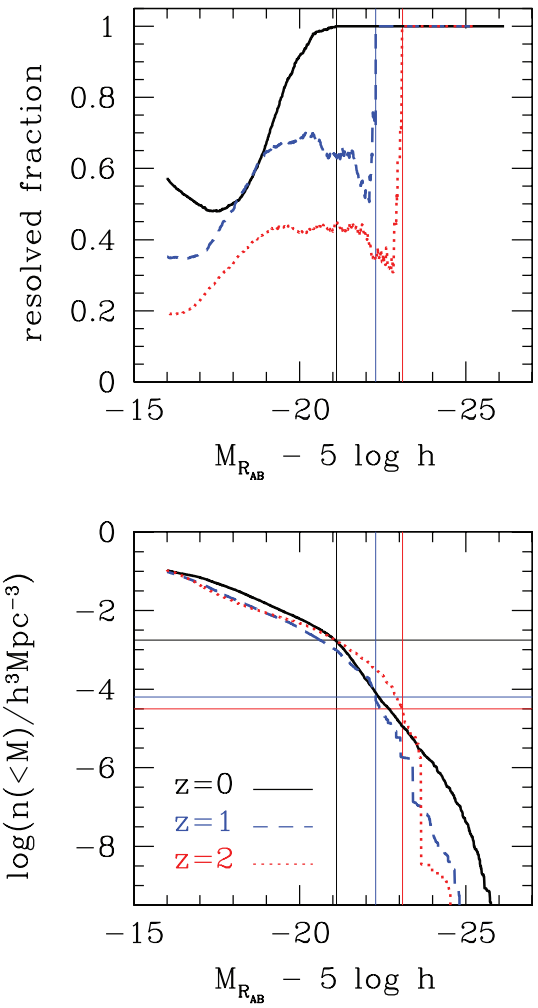

Figure 4. Upper panel: the fraction of 'resolved galaxies' in the high-resolution *N*-body simulation as a function of magnitude, at different output redshifts (as given by the key in the lower panel). The magnitude is in the observer-frame *R* band; to obtain an apparent *R*-band magnitude, the distance modulus corresponding to the redshift should be added to the plotted magnitude. The vertical lines mark the magnitude at which the galaxy sample is 100 per cent complete at each redshift. Lower panel: the cumulative luminosity function of galaxies brighter than a given *R*-band magnitude, for different redshifts as given in the key. The vertical lines show the 100 per cent completeness limits at each redshift and the horizontal lines indicate the associated space density of galaxies.

3 THE POWER SPECTRUM OF GALAXY CLUSTERING

In this section we examine the various phenomena which are responsible for changing the form of the power spectrum of galaxy clustering from that expected in linear perturbation theory. We systematically add in new effects and elements of sample selection, considering first the power spectrum of the dark matter, looking at non-linear evolution (Section 3.1) and the impact of peculiar velocities (Section 3.2), before moving on to dark matter haloes (Section 3.3) and finally to synthetic galaxy samples (Section 3.4).

For completeness, we first explain some of the terminology we use in this section. There are three types of phenomena responsible for distorting the linear theory power spectrum: (i) non-linear growth of fluctuations, (ii) redshift-space distortions and (iii) bias. Non-linear growth refers to the coupled evolution of density fluctuations on different scales. Redshift-space distortions describe the impact of gravitationally induced peculiar motions on the clustering pattern. We will refer to clustering measurements as being made in 'real space' or 'redshift space'; in the latter case peculiar motions are taken into account, as we describe in Section 3.2. The term 'bias' has a range of meanings in the literature. Bias is used to describe the boost in the clustering of a particular tracer (e.g. galaxies or clusters) relative to a reference point, which could be the clustering of the dark matter in either linear perturbation theory or taking into account non-linear evolution. One of the earliest uses of the concept of bias was in the application of the high-peak model to explain the enhanced clustering of Abell clusters (Kaiser 1984). In this model, clusters are associated with rare peaks in the initial, Gaussian density field. The bias is defined as the square root of the ratio of the two-point correlation function of peaks of a certain minimum height to the clustering of the mass expected in linear perturbation theory. When considering galaxies, it is perhaps more natural to think in terms of a modulation of clustering relative to that displayed by the underlying mass at the same epoch, since galaxies populate dark matter haloes. In this case, the galaxy clustering will be measured relative to that of the evolved matter distribution. On large scales, these two reference points, the clustering of the matter expected in linear perturbation theory or the evolved clustering, should be essentially the same. We shall see later that this is approximately the case for the scales over which we compare clustering signals to measure bias factors.

3.1 The non-linear growth of matter fluctuations

The early stages of the growth of a density fluctuation are particularly simple to describe analytically. The fluid equations can be written in terms of the perturbation to the density and Fourier transformed. In the simplest case, when the density contrast $\delta \ll 1$, the Fourier modes evolve independently of one another. This is called linear growth. In this regime, the power spectrum changes in amplitude with time, but not in shape. The shift in amplitude is described by the growth factor D, which is a function of the densities of matter and dark energy (as quantified by the present-day density parameters, $\Omega_{\rm M}$ and Ω_Λ, for matter and dark energy, respectively) and redshift (see Heath 1977; Peebles 1980):

$$P(k, z) = D^2(z, \Omega_{\rm M}, \Omega_\Lambda) P(k, z = 0), \quad (4)$$

where $D(z = 0) = 1$.

We plot the power spectrum of the dark matter in real space measured from the BASICC at different output redshifts in Fig. 5. The approximately linear growth of the power spectrum is readily apparent on large scales (low k). In an Einstein–de Sitter universe ($\Omega_{\rm M} = 1$), the growth factor is equal to the expansion factor. If dark energy plays a role in setting the rate at which the Universe expands, the growth of fluctuations is suppressed relative to the Einstein–de Sitter case at late times. The BASICC started at $z_{\rm s} = 63$, so if $\Omega_{\rm M} = 1$, we would expect to see the power spectrum grow in amplitude by a factor of $(1 + z_{\rm s})^2 = 4096$ by $z = 0$. Using the approximate formula provided by Carroll, Press & Turner (1992), we expect a suppression in the growth of the power by a factor of 0.5537 for the cosmological parameters used in the simulation. This gives an overall growth in power from the initial conditions to the present of a factor of 2268. This agrees to within 0.6 per cent with the factor expected from a direct numerical integration of the equation giving the growth factor (equations 28 and 9 from Carroll et al. 1992), which gives 2281.01. In the simulation, we find that the power in the fundamental mode grows by a factor of 2285.21 from the initial

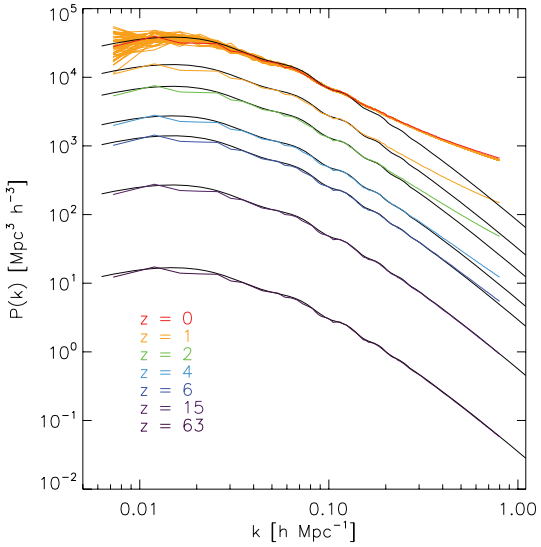

Figure 5. The growth of the power spectrum of density fluctuations in the dark matter, as measured in real space. The smooth curves show the predictions of linear perturbation theory at the redshifts indicated by the key. The power spectra measured in the low-resolution ensemble at $z = 0$ are plotted to show the sampling variance for a simulation box of side $1340\,h^{-1}$ Mpc. The smallest wavenumber plotted corresponds to the fundamental mode in the simulation, $2\pi/L = 0.0469\,h^{-1}$ Mpc. The maximum wavenumber shown is 0.67 times the Nyquist frequency of the FFT grid, chosen to avoid any aliasing effects.

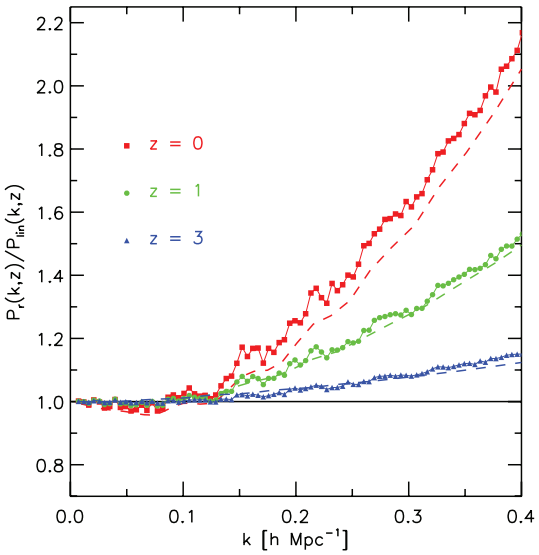

Figure 6. The non-linear growth of the power spectrum. Here we divide the power spectrum in real space measured at the redshift indicated by the key by the power spectrum at $z = 15$, after taking into account the change in the growth factor. Any deviation of the resulting ratio from unity indicates a departure from linear perturbation theory. The dashed lines show the same ratio as predicted using the ansatz of Smith et al. (2003).

conditions at $z = 63$–0, which agrees with the growth predicted by linear perturbation theory to 0.02 per cent.

Fig. 5 shows that the growth of the power spectrum is clearly not linear at high wavenumbers. The shape of the spectrum at high k at late times is different from that at high redshift, because the growth of modes of different k becomes coupled. This behaviour can be followed to some extent using second-order and higher order perturbation theory (Peebles 1980; Baugh & Efstathiou 1994; Jain & Bertschinger 1994; Crocce & Scoccimarro 2006b). However, as the density contrast approaches unity, second-order perturbation theory breaks down (Baugh & Efstathiou 1994). The coupled evolution of the Fourier modes starts on surprisingly large scales, which demonstrates the necessity of a large volume simulation to accurately follow the development of the power spectrum (Smith, Scoccimarro & Sheth 2007). This can be seen more clearly if we divide the measured spectrum by the growth expected according to linear perturbation theory, as is done approximately in Fig. 6. In this plot, we have divided the power spectra measured from the simulation by the spectrum measured at $z = 15$, scaled by the square of the appropriate growth factor. This reduces the noise in the ratio arising from the finite number of modes realized at small wavenumbers in the simulation volume (Baugh & Efstathiou 1994; Springel et al. 2005). Any deviation away from unity signifies a departure from linear perturbation theory due to coupling between modes. The ratio shows a characteristic dip at low k, i.e. less power than expected in linear theory, before showing a strong enhancement at higher wavenumbers (Baugh & Efstathiou 1994). It is remarkable that the transition between a deficit and excess of power happens at the same wavenumber, $k \sim 0.1\,h\,\mathrm{Mpc}^{-1}$, at different epochs. The suppression in power at low k, on the order of a 3 per cent, is not as strong as that seen in an Einstein–de Sitter universe (see fig. 4 of Baugh & Efstathiou 1994). Nevertheless, this drives the spectacular boost in power seen at higher wavenumbers. The dip in power is largest around $k \sim 0.05\,h\,\mathrm{Mpc}^{-1}$, which corresponds to a length-scale of $2\,\pi/k \sim 125\,h^{-1}$ Mpc, close to the wavelength of the acoustic oscillations. Several authors have proposed ansatzes which transform the linear perturbation theory power spectrum into the non-linear power spectrum (e.g. Hamilton et al. 1991; Peacock & Dodds 1994, 1996; Smith et al. 2003). We plot the predictions of the model proposed by Smith et al. (2003) in Fig. 6 using dashed lines. The ratio is computed by dividing the power spectrum at the epoch of interest by the suitably scaled prediction of the model for $z = 15$. The agreement is excellent at high redshift. At $z = 0$, at higher wavenumbers, the Smith et al. (2003) formula recovers the simulation results to within 5 per cent over the range plotted.

3.2 The impact of redshift-space distortions on the power spectrum

In a spectroscopic galaxy survey, the radial distance to an object is inferred from its measured redshift. The shift in the spectral features of the galaxy is produced by two contributions to its the apparent velocity: the expansion of the Universe, which is responsible for the Hubble flow at the true distance to the galaxy, and local inhomogeneities in the gravitational field around the object, which generate an additional, 'peculiar' velocity. Since we cannot correct a priori for the effects of the local gravitational field when inferring the radial distance from the Hubble law and the measured redshift, an error is made in the distance determination. The impact of such errors on the form of the measured power spectrum of clustering is called the redshift-space distortion.

Peculiar motions display two extremes which produce different types of distortion to the power spectrum. (i) On large scales, coherent bulk flows out of voids and into overdense regions lead to an enhancement in the density inferred in redshift space, and hence to a boost in the recovered power. Kaiser (1987) derived a formula for the enhancement of the spherically averaged power, under the assumption of linear perturbation theory for an observer situated at

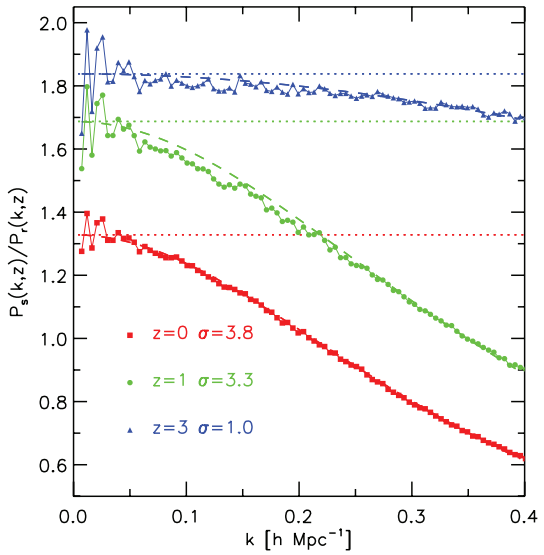

Figure 7. The ratio of the power spectrum measured for the dark matter in redshift space, i.e. including the impact of peculiar motions in the distance determination, to the power spectrum measured in real space. The deviation from unity shows the redshift-space distortion to the non-linear power spectrum. The results are shown for selected output redshifts, as indicated by the key. The horizontal dotted lines indicate the boost in the redshift-space power expected due to coherent flows, as predicted by equation (5). The dashed lines show a simple fit to the distortions (see equation 6).

infinity (the plane parallel approximation):

$$f = \frac{P_s(k)}{P_r(k)} = \left(1 + \frac{2}{3}\beta + \frac{1}{5}\beta^2\right), \quad (5)$$

where $P_s(k)$ is the power spectrum in redshift space, $P_r(k)$ is the spectrum in real space and $\beta = (\mathrm{d}\log\delta/\mathrm{d}\log a)/b \simeq \Omega_M^{0.6}(z)/b$, where b is the bias factor ($b = 1$ for the dark matter; for a discussion of the dependence of the growth factor on Ω_M, see Linder 2005; Linder & Cahn 2007). (ii) On small scales, the random motions of objects inside virialized dark matter haloes cause structures to appear elongated when viewed in redshift space, leading to a damping of the power. Peacock & Dodds (1994) discussed a model for the redshift-space power spectrum, which takes into account both limits of peculiar motions (see also Scoccimarro 2004).

Fig. 7 shows the ratio of the power spectrum measured for the dark matter in redshift space to that measured in real space, at redshifts $z = 3, 1$ and 0. The dotted lines indicate the boost expected in the redshift-space power, computed using the expression in equation (5) (Kaiser 1987). This factor changes with redshift because the matter density parameter is changing. Fig. 7 shows that this behaviour is only approached asymptotically, on scales in excess of $100\,h^{-1}$ Mpc. At higher wavenumbers, the power measured in redshift space is suppressed by random motions. The dashed lines in this plot show a simple fit to this ratio

$$f = \frac{P_s(k)}{P_r(k)} = \left(1 + \frac{2}{3}\beta + \frac{1}{5}\beta^2\right)\left(1 + k^2\sigma^2\right)^{-1}, \quad (6)$$

where σ is a free parameter, which is loosely connected to the pairwise velocity dispersion. The degree of damping grows between $z = 3$ and 1, but changes relatively little by $z = 0$. We shall see in later sections that the form of the redshift-space distortion to the power spectrum depends on the type of object under consideration.

3.3 The power spectrum of dark matter haloes in real and redshift space

In modern theories of galaxy formation, dark matter haloes play host to galaxies. It is therefore instructive to compare the power spectra measured for different samples of haloes to that of the dark matter as a step towards understanding the power spectrum of galaxies.

A common conception is that the clustering of haloes is a scaled version of the clustering of the underlying mass, with the shift in clustering amplitude quantified in terms of a bias factor, b, where $b^2 = P_{\rm haloes}/P_{\rm dm}$ (Cole & Kaiser 1989; Mo & White 1996). As we commented earlier, since we use the dark matter power spectrum on large scales to define a bias, this is approximately the same as using the linear perturbation theory spectrum. Many authors have tested analytical prescriptions for computing the bias parameter using extensions of the theory of Press & Schechter (1974) (e.g. Mo, Jing & White 1997; Sheth, Mo & Tormen 2001; Jing 1998; Governato et al. 1999; Colberg et al. 2000; Seljak & Warren 2004). In the extended Press–Schechter theory, the bias is only a function of halo mass and redshift. However, recent analyses of high-resolution, large volume simulations have revealed some dependence of halo clustering on a second parameter besides mass, such as the halo's formation redshift or concentration parameter (Gao et al. 2005; Harker et al. 2006; Wechsler et al. 2006).

In Fig. 8, we show that this simple picture, in which the clustering of haloes is a shifted version of that of the dark matter, is actually a poor approximation to what we find in the simulation. We show the ratio of the power spectrum of a sample of dark matter haloes measured in real space to a scaled version of the linear perturbation theory power spectrum. The amplitude of the linear theory spectrum used in the ratio takes into account the growth factor appropriate to the output redshift and an effective bias, which is set by matching the linear theory prediction for the mass spectrum to the measured halo spectrum on large scales, i.e. for wavenumbers in the range $0.0046 < k\,(h\,\mathrm{Mpc}^{-1}) < 0.1$. Each panel in Fig. 8 corresponds to a different output redshift from the simulation. For each redshift, we have defined three samples of dark matter haloes, which contain the same number of objects. The mass intervals are set relative to the average halo mass present in the respective outputs, with 'low', 'mean' and 'high' mass samples considered. Each of these contains 20 per cent of the total number of haloes present at each epoch, with the mass ranges used at each redshift indicated on the keys. The effective bias factors of the halo samples are also written in the key. For comparison, the dashed line in each panel shows the corresponding ratio for the dark matter.

Fig. 8 shows that at $z = 3$, all of the haloes considered have effective biases much greater than unity, indicating they are more strongly clustered than the mass. This situation is reversed at $z = 0$. At this epoch, the halo mass resolution of the BASICC is smaller than the corresponding value of M_*[1] ($=5.78 \times 10^{12}\,h^{-1}\,\mathrm{M}_\odot$ at $z = 0$). The $z = 0$ samples have a bias of unity or smaller. In addition to the difference in the effective bias parameters, the shape of the spectrum of the haloes in these extremes is also different (see also Smith et al. 2007). The plot shows the shape of the power spectrum, after accounting for the effective bias on large scales. Any difference between the curves plotted for the haloes and that for the dark matter (dashed line) shows a difference in the clustering signal over and

[1] M_* is a characteristic mass scale defined as the mass within a sphere for which the rms variance in linear perturbation theory is $\sigma(M) = \delta_{\rm crit}(z)$, where $\delta_{\rm crit}$ is the extrapolated critical linear overdensity given by the spherical collapse model at redshift z.

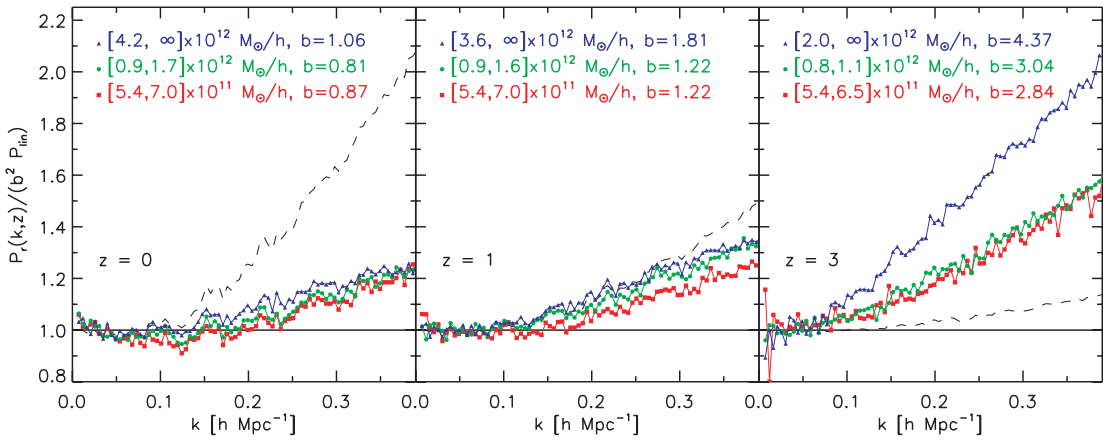

Figure 8. The power spectrum of dark matter haloes measured in real space compared to a scaled version of the prediction of linear perturbation theory, which takes into account the growth factor and an effective bias computed on large scales $k < 0.1\,h\,\mathrm{Mpc}^{-1}$. Each panel corresponds to a different output redshift. Different mass samples are considered, as indicated by the key, which correspond to low, average and high masses, defined in terms of the average halo mass present at each output time. The black dashed line shows the real-space power spectrum of the mass divided by the appropriate linear perturbation theory prediction.

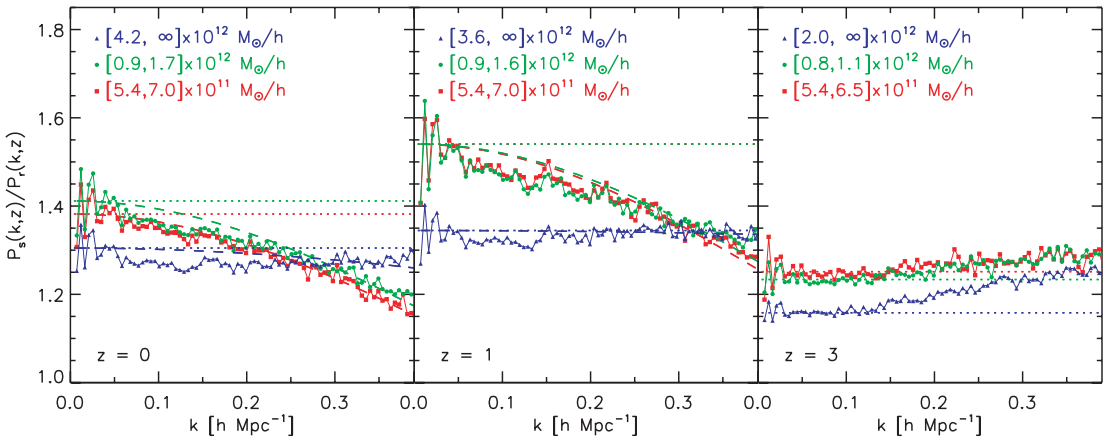

Figure 9. The power spectrum of dark matter haloes measured in redshift space divided by the power spectrum measured in real space for the same sample. Each panel corresponds to a different output redshift. Different mass samples are considered, as indicated by the key, which correspond to low, average and high masses, defined in terms of the average halo mass present at each output time. The horizontal dotted lines show the expected ratio for the boost in the amplitude of the redshift-space power spectrum due to coherent flows, computed using an effective bias factor estimated on large scales. The dashed lines show the best-fitting model of equation (6), which turns out to be a poor description of the redshift-space distortions. No suitable fits were obtained at $z = 3$.

above that quantified by a constant effective bias. Similar behaviour was found for samples of cluster mass haloes in the Hubble Volume Simulation by Angulo et al. (2005).

We now consider the clustering of haloes as viewed in redshift space, taking the centre of mass velocity of the halo as its peculiar velocity. In Fig. 9, we plot the ratio of the redshift-space power spectrum for the halo samples used in Fig. 8 to the power spectrum measured in real space. As we did before for the case of the dark matter (Fig. 7), we indicate the boost in power expected on large scales (small k) due to coherent bulk flows of haloes. The boost is calculated from equation (5) using the effective bias of the halo sample. The plot shows that the redshift-space power spectrum at low wavenumbers is in reasonable agreement with this simple model. However, a range of behaviour is seen at higher wavenumbers. For haloes comparable to M_*, the boost in power in redshift space is less than predicted by equation (5). For the more extreme, massive haloes, there is actually more power in redshift space than is suggested by Kaiser's formula. This 'excess' power was previously noted by Padilla & Baugh (2002) and Angulo et al. (2005). The Kaiser formula assumes linear perturbation theory and breaks down in the case of objects with strongly non-linear clustering. In the case of the less extreme haloes, the reduction in power is *not* due to virialized motions of haloes within larger structures. The halo finder we have used is designed to return an overdensity corresponding to virialized structures and not substructures. If the haloes were really part of a larger structure and were executing random motions, the group finder would simply have lumped them together as one larger structure. We are perhaps seeing instead haloes that have started to merge with one another, and whose motions have broken away from a coherent large-scale flow. We know of no analytical description of the redshift-space clustering of dark matter haloes which explains this behaviour.

3.4 The power spectrum of galaxies

The galaxy power spectrum can be very different from the power spectrum of a sample of dark matter haloes. The way in which the galaxies are distributed among haloes changes the form of the power

spectrum. In a mass-limited sample of haloes, the contribution of each halo to the power spectrum can be determined through its space density, which acts as a weighting factor when computing the contribution of the halo to the clustering signal. The number of galaxies per halo acts to modify this weight, e.g. more massive haloes could contain more galaxies than less massive haloes. Furthermore, the presence of satellite galaxies within a halo means that one expects to see a damping in power on small scales in redshift space, due to the random motions of the satellites within the virialized dark halo. The precise modification of the power spectrum depends in detail on how galaxies populate dark matter haloes. As we discussed in Section 2.2, we have carried out an *ab initio* calculation of the number of galaxies per halo, using a semi-analytic model of galaxy formation. We are able to predict observable properties of galaxies, such as broad-band magnitudes and the strength of emission lines. We consider a range of galaxy samples, defined either by a magnitude limit alone (set in the R band) or by combining an R-band magnitude limit with a colour selection (in $R - I$) or a cut on the strength of the O II[3727] emission line.

(i) Sample A: magnitude limited to reach a space density of $5 \times 10^{-4}\,h^3\,\mathrm{Mpc}^{-3}$.
(ii) Sample B: magnitude limited to reach half the space density of sample A, i.e. $2.5 \times 10^{-4}\,h^3\,\mathrm{Mpc}^{-3}$.
(iii) Sample C: the reddest 50 per cent of galaxies from sample A, using the $R - I$ colour.
(iv) Sample D: the 50 per cent of galaxies from sample A with the strongest emission lines, using the equivalent width of O II[3727].
(v) Sample E: the bluest 50 per cent of galaxies from sample A, using the $R - I$ colour.
(vi) Sample F: the 50 per cent of galaxies from sample A with the weakest emission lines, using the equivalent width of O II[3727].

The power spectra measured in real space from the various galaxy samples are plotted in Fig. 10. The spectra have been divided by the linear perturbation theory power spectrum multiplied by the square of an effective bias factor, which was estimated by comparing the galaxy spectra to the power spectrum measured for the dark matter for wavenumbers $k < 0.1\,h\,\mathrm{Mpc}^{-1}$. In all cases, for the space densities we have chosen, the effective bias factors estimated for the samples are modest. For comparison, the ratio of the power spectrum of the dark matter in real space to the linear theory prediction is also plotted, using a dashed line. The deviation of the dashed line from unity shows where non-linear effects are important for the dark matter. Any differences between the plotted ratios for galaxies and mass indicate a scale-dependent bias. The comparison between the dashed and solid curves in Fig. 10 shows that a constant bias is only a good approximation on large scales, $k < 0.15\,h\,\mathrm{Mpc}^{-1}$.

The redshift-space distortion in the galaxy power spectrum is shown in Fig. 11, where we plot the ratio of the redshift-space spectrum to the real-space spectrum for the galaxy samples shown in Fig. 10. The horizontal lines show the Kaiser boost (equation 5) expected for the effective bias of the galaxy sample. This ratio is only attained on the very largest scales and seems to be an overestimate of the size of the effect at $z = 1$. The damping of the power on intermediate and small scales is readily apparent and, unlike the case with dark matter haloes, is well described by the form given in equation (6).

4 CONSTRAINING THE DARK ENERGY EQUATION OF STATE

In this section we outline the procedures we follow to place constraints on the dark energy equation of state parameter, w, by measuring the length-scale imprinted by BAO on the power spectrum of the various tracers of the density field. The transformation of a measurement of a distance scale into a constraint on w requires various approximations to be made, and depends upon the survey in question and upon the time variation assumed for the dark energy. Nevertheless it is instructive to go through this exercise, bearing these caveats in mind, to get a feel for how well future experiments will be able to measure w for the case of a constant equation of state.

The form of the power spectrum of density fluctuations contains information about basic cosmological parameters, and measurements of the galaxy power spectrum on large scales have been exploited to extract the values of these parameters (e.g. Cole et al. 2005; Sánchez et al. 2006; Tegmark et al. 2006; Padmanabhan et al. 2007;

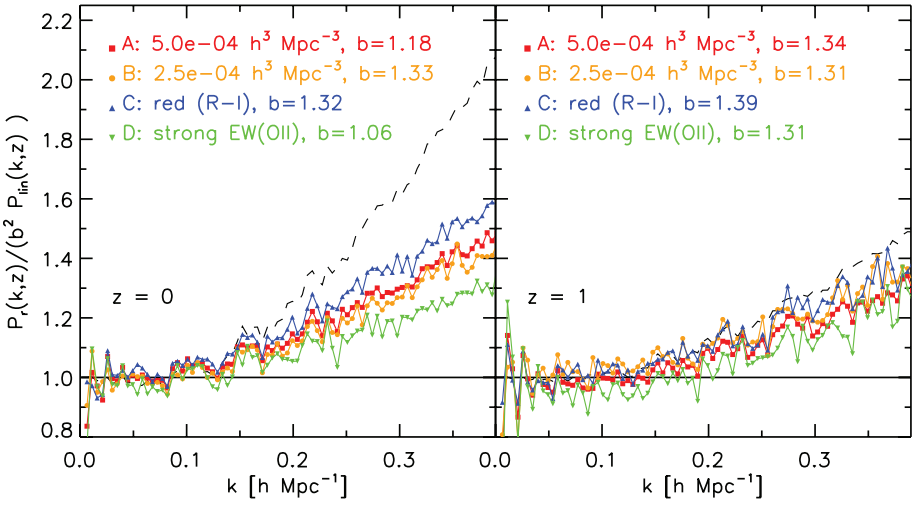

Figure 10. The power spectrum of different galaxy samples measured in real space, divided by the square of an effective bias parameter and the appropriately scaled linear perturbation theory power spectrum. The sample definition and the value of the effective bias used are given by the key. The power spectrum of the dark matter spectrum in real space, also divided by the linear perturbation theory spectrum, is shown by the black dashed line. The left-hand panel shows the ratios at $z = 0$ and the right-hand panel at $z = 1$.

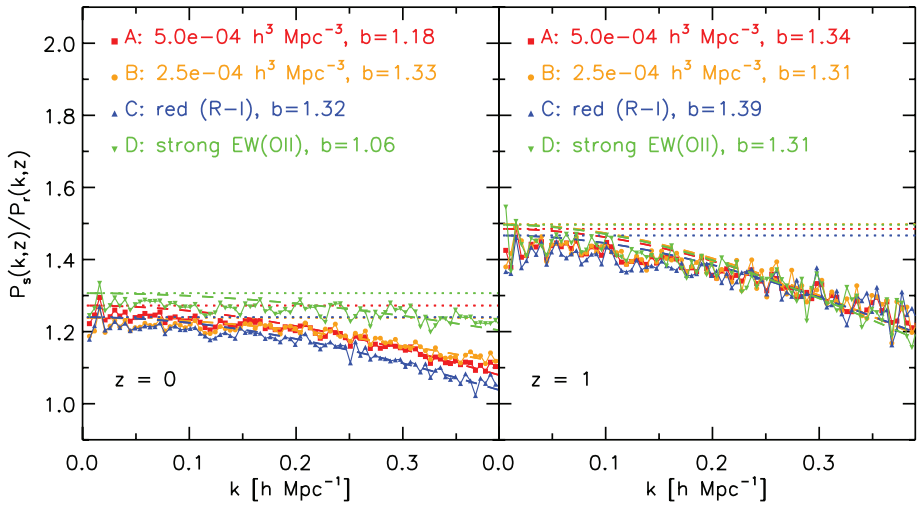

Figure 11. The ratio of the power spectrum of galaxies measured in redshift space to that in real space, at $z = 0$ (left-hand panel) and $z = 1$ (right-hand panel). The samples are defined by the key in each panel. The dotted horizontal lines show the predictions of equation (5) for the various samples.

Percival et al. 2007). The apparent scale of features in the power spectrum offers another route to constrain selected cosmological parameters through the dependence of the distances parallel and perpendicular to the line of sight on the matter density parameter, $\Omega_{\rm M}$, the dark energy density parameter, $\Omega_{\rm DE}$, the dark energy equation of state parameter, w and the Hubble constant. For such an approach to work, we either need to know the true physical scale of a particular feature in the power spectrum beforehand or to compare the relative size of a feature when measured parallel and perpendicular to the line of sight (Alcock & Paczynski 1979). The baryonic oscillations present a promising candidate for such a feature. If we assume for the sake of argument that the cosmological parameters, apart from the equation of state of the dark energy, are well constrained, then the scale of the acoustic oscillations becomes a standard ruler. These features are expected on smaller scales than the turnover and have already been seen in current surveys at low redshift, although at too low a signal-to-noise ratio to use in isolation to extract a competitive constraint on the dark energy equation of state (Cole et al. 2005; Eisenstein et al. 2005).

We can see how the value of the equation of state parameter of the dark energy influences the form of the BAO with the following simple argument. To measure the power spectrum of galaxy clustering, we need to convert the angular positions and redshifts of the galaxies into comoving spatial separations. This requires a choice to be made for values of the cosmological parameters, including w. In our case, we set the parameters equal to the values used in the N-body simulations, with $w = w_{\rm true} = -1$ for the particular case we have run. The effect of a change in the value of w, $w_{\rm assumed} = w_{\rm true} + \delta w$ is to change the separations between pairs of galaxies, which leads to a change in the appearance of the power spectrum. For small perturbations away from the true equation of state, we assume that the alteration in the measured power spectrum can be represented by a rescaling of the wavenumber from $k_{\rm true}$ to $k_{\rm app}$. The ratio of these wavenumbers gives a 'stretch' parameter, α, which describes the change in the recovered oscillation scale:

$$\alpha = \frac{k_{\rm app}}{k_{\rm true}}. \tag{7}$$

If $w_{\rm assumed} = w_{\rm true}$, then there is no shift in the BAO in the estimated power spectrum and $\alpha = 1$. In the case of a wide-angle, deep galaxy survey with spectroscopic redshifts, the stretch parameter can be approximated by

$$\alpha \approx \left[\frac{D_{\rm A}(z, w_{\rm assumed})}{D_{\rm A}(z, w_{\rm true})}\right]^{-2/3} \left[\frac{H(z, w_{\rm true})}{H(z, w_{\rm assumed})}\right]^{1/3}, \tag{8}$$

where

$$H(z, w) = H_0[\Omega_{\rm m}(1+z)^3 + \Omega_{\rm DE}(1+z)^{3(1+w)}]^{1/2}, \tag{9}$$

$$D_{\rm A}(z, w) = \frac{c}{1+z}\int_0^z \frac{{\rm d}z}{H(z)}. \tag{10}$$

The values of the exponents in equation (8), 2/3 for the distance transverse to the line of sight and 1/3 for the distance parallel to the line of sight are motivated by the number of Cartesian components in these directions (e.g. Eisenstein et al. 2005). The precise value of these exponents will depend upon the geometry and construction of the galaxy survey. For example, in a survey which relies upon photometric redshifts, the exponent parallel to the line of sight would be greatly reduced and it would be beneficial to compute the power spectrum transverse to the line of sight. Note that in equations (9) and (10) we assume that w is independent of redshift. There are many models in which w is a function of redshift. In this case, the exponent of $\Omega_{\rm DE}$ in the expression for the Hubble parameter (equation 9) would be replaced by an integral over $w(z)$.

It is instructive to see how the constraints on α translate into limits on the value of w. We can do this approximately using equation (8), for the case of a redshift independent equation of state, considering perturbations around $w_{\rm true} = -1$. We consider two illustrative cases: a 'pessimistic' case in which we consider the constraints from BAO in isolation from any other data which constrain the cosmological parameters and an 'optimistic' case, in which we perturb w and only consider cosmological models that give similar predictions for the CMB.[2] The translation in the pessimistic case is shown in the upper panel of Fig. 12 for two different redshifts. Here we have assumed fixed values for $\Omega_{\rm M}$ and Ω_Λ and we have not marginalized over

[2] We acknowledge the referee for suggesting this second case to us and for encouraging us to perform the calculation.

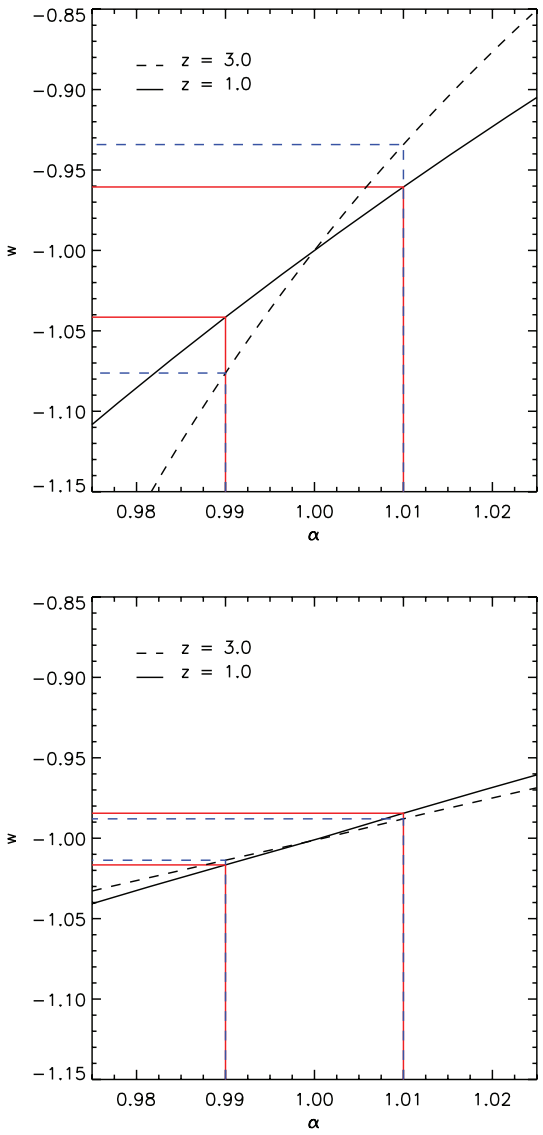

Figure 12. The relation between the dark energy equation of state parameter, w, and the scalefactor, α, defined by equation (8), for perturbations in the equation of state around $w_{\rm true} = -1$. Two cases are shown. In the upper panel, the values of the other cosmological parameters are kept fixed. In the lower panel, the ratio of the sound horizon scale to the angular diameter distance to the last scattering surface is held fixed. The relation between α and w is shown for $z = 1$ (solid lines) and $z = 3$ (dashed lines). The horizontal and vertical lines guide the eye to show how a 1 per cent error in α translates into an error in w.

these parameters. This is the case discussed most commonly in the literature. Under these conditions, at $z = 1$, a 1 per cent error in α corresponds approximately to a 4 per cent error in the value of w. At $z = 3$, the boost is about 50 per cent larger, with $\delta w \approx 6\delta\alpha$.

In the 'optimistic' case, we only consider models which give the same angular location for the first peak in the CMB spectrum. Hence, when the value of w is perturbed, we restrict our attention to those models which give the same ratio of the sound horizon scale to the angular diameter distance to the last scattering surface as our default cosmology. Given the parametric forms quoted for these distances by Eisenstein & Hu (1998), this is equivalent to keeping $\Omega_{\rm b}/\Omega_{\rm M}$ and h fixed, and varying $\Omega_{\rm M}$. We have called this case 'optimistic' because it does not include any error on the fixed parameters. In this scenario, shown in the lower panel of Fig. 12, the error on w is now only around 50 per cent larger than the corresponding error on α.

We now explore two of the approaches which have been advocated in the literature to measure the value of w. Both methods involve making fits to the ratio of a measured power spectrum divided by a smooth reference spectrum. In the first approach, a parametric form is assumed for the ratio (Blake & Glazebrook 2003). The second approach is more general as it does not assume a specific form for the ratio, but instead uses the linear perturbation theory power spectrum without any further approximations (Percival et al. 2007; see also Eisenstein et al. 2005). We shall henceforth refer to these methods as the parametric and general schemes, respectively. In their original forms, there are also differences in the way in which a 'featureless' reference spectrum is constructed, as we will briefly discuss when describing these approaches below.

Blake & Glazebrook (2003; see also Glazebrook & Blake 2005) studied the feasibility of extracting measurements of the acoustic oscillations from forthcoming galaxy surveys using linear perturbation theory. Their starting point is to divide the power spectrum, including the imprint of baryons, divided by a smooth reference spectrum which is chosen to be free from any signature of acoustic oscillations. This method therefore does not use any of the information contained in the overall shape of the power spectrum, which Blake & Glazebrook argue could be susceptible to large-scale gradients arising from the effects we discussed in Section 3, such as galaxy bias or redshift-space distortions. Instead, they focused on the location and amplitude of the acoustic oscillations. The smooth reference spectrum is obtained using the zero-baryon transfer function written down by Eisenstein & Hu (1998). The parametric form suggested by Blake & Glazebrook as a fit to the resulting ratio is a Taylor expansion of the ratio of a power spectrum for CDM plus a small baryonic component, divided by a pure CDM power spectrum. The sound horizon, which is a free parameter in their method, is treated as the oscillation wavelength in this parametric form. This is an approximation, as the wavelength of the acoustic oscillations actually changes with wavenumber, albeit slowly, and is therefore not a constant (see equation 22 of Eisenstein & Hu 1998). Some authors have criticized this approach due to the sensitivity of the ratio to the choice of the reference power spectrum. Angulo et al. (2005) describe how realistic power spectra, which include non-linear growth, bias effects and redshift-space distortions, require a 'linearization' process before they become adequately described by the parametric form put forward by Blake & Glazebrook. Due to the sensitivity of the ratio to the choice of reference spectrum at low wavenumbers, Koehler et al. (2007) proposed ignoring power-spectrum measurements below $k \sim 0.05\,h\,{\rm Mpc}^{-1}$ to avoid this problem (although we note that they also discuss a different approach to measuring the equation of state parameter).

Percival et al. (2007) proposed a new technique which has a number of appealing features compared with that of Blake & Glazebrook. First, the shortcut of fitting an approximate parametric form to the ratio of the measured power spectrum to a reference is dropped in favour of using a full linear perturbation theory power spectrum (with a modification; see later) to model the ratio. This is completely general, and permits one to use the most accurate description available of the linear perturbation theory power spectrum, such as the tabulated output of CAMB. Secondly, the reference power spectrum is defined separately in the case of the data and the linear theory model, by using a coarse rebinning of the relevant power spectrum. The reference is constructed using a spline fit to a reduced number of wavenumber bins over the range in which the spectrum in question is defined. Thus, any deviations in the general form of the measured

spectrum away from linear theory are naturally accounted for in the reference spectrum. Thirdly, Percival et al. allow for a damping of the amplitude of the oscillations in the theoretical ratio beyond some wavenumber, which is treated as a free parameter in their fit. The quality of the fits is dramatically improved when damping of the higher harmonics is allowed. Percival et al. applied their method to extract the matter density parameter from the power spectrum of LRGs in the SDSS.

The majority of the results we present are obtained using the general method suggested by Percival et al. For completeness, and because Percival et al. did not actually apply their method to the extraction of the equation of state parameter, we set out the general approach step by step below.

(1) A smooth reference spectrum (i.e. without any oscillatory features), $P_{\rm ref}$, is constructed from the measured power spectrum using a cubic spline fit over the wavenumber range $0.0046 < k(h\,{\rm Mpc}^{-1}) < 1.2$, using the measured spectrum smoothed over 25 bins in wavenumber. The spline is constrained to pass through the data points in this coarse rebinning of the measured power spectrum.

(2) We compute the ratio, R(k), of the measured power spectrum, $P(k)$, to the reference spectrum, $P_{\rm ref}(k)$, obtained in step 1:

$$R(k) = \frac{P(k)}{P_{\rm ref}(k)}. \tag{11}$$

(3) A linear perturbation theory power spectrum is generated with CAMB for the cosmological parameters used in the BASICC simulation. A smooth reference spectrum, $P^{\rm L}_{\rm ref}$, is defined for this spectrum in the same manner as described for the measured spectrum in step 1, using the same wavenumber bins. A ratio, $R_{\rm L}$, is derived for the linear perturbation theory spectrum by dividing by this reference spectrum.

(4) The linear theory ratio, $R_{\rm L}$, is compared with the measured ratio, R. Two modifications are considered to the linear theory ratio. The first is a stretch or scaling of the wavenumber used in the linear theory ratio, as described above, to mimic the act of changing the dark energy equation of state parameter, w. The goal here is to see what variation in w can be tolerated before $R_{\rm L}$ is no longer a good fit to the measured ratio R. The second change is to allow for a damping of the oscillations beyond some characteristic wavenumber by multiplying the theoretical power spectrum by a Gaussian filter:

$$W(k) = \exp\left(-\frac{k^2}{2k_{\rm nl}^2}\right), \tag{12}$$

where $k_{\rm nl}$ is a free parameter. Hence, the linear theory ratio is modified to

$$R_{\rm L}(k) = \left[\frac{P^L}{P^L_{\rm ref}}(\alpha k) - 1\right] W(k, k_{\rm nl}) + 1. \tag{13}$$

(5) A likelihood is computed for each combination of the parameters $k_{\rm nl}$ and α, assuming Gaussian errors:

$$-2\ln L = \chi^2 = \sum_i \left(\frac{R^i - R^i_{\rm L}}{\sigma^i / P^i}\right)^2, \tag{14}$$

where the summation is over wavenumber and σ^i is the error on the power spectrum estimated in the $i^{\rm th}$ bin (as given by equation 3). We generate a grid of models using 200^2 different combinations of α and $k_{\rm nl}$ in the ranges [0.9, 1.1] and [0, 0.4], respectively.

(6) Finally, the best-fitting values for α and $k_{\rm nl}$ correspond to those for the model with the maximum likelihood. We obtain confidence limits on the parameter estimation by considering the models within $\Delta\chi^2$ equal to 2.3 and 6.0; in the case of a Gaussian likelihood, these would correspond to the 68 per cent (1σ error) and 95 per cent (2σ error) confidence levels on the best fit. We note that in some cases presented later (see Fig. 15), the distribution of the likelihood is not Gaussian.

In some cases, we also present constraints on w derived using a slightly modified version of the approach of Blake & Glazebrook. The main difference is that we follow step 1 to construct a ratio from the measured power spectrum, rather than using a zero-baryon transfer function.

One issue to be resolved is the range of wavenumbers which should be used in the fitting process. To address this, we used the power spectrum of the dark matter measured at $z = 6$. We systematically varied the minimum and maximum wavenumbers used in our fit and compared the values of the scaling parameter, α, recovered. Our results are fairly insensitive to the choice of the maximum wavenumber, particularly when damping of the oscillations is included in the fitting algorithm. However, the recovered α shows a systematic shift once the minimum wavenumber exceeds $k \sim 0.1\,h\,{\rm Mpc}^{-1}$. For minimum wavenumbers smaller than this, there is little difference in the recovered value of α or in the size of the errors on α, as these modes have relatively large errors in our simulation. This is encouraging news for realistic survey geometries, for which the power spectrum measured at low wavenumbers will be distorted due to the window function of the survey. In the rest of the paper, we use the power spectrum in the wavenumber interval $k(h\,{\rm Mpc}^{-1}) = [0, 0.4]$ to constrain the value of α.

5 RESULTS

In this section, we present the expected constraints on the dark matter equation of state using the power spectra measured from our simulations. We first show how our algorithm for extracting the equation of state parameter works in practice, for dark matter particles, haloes and galaxies, comparing the results obtained in real and redshift space (Section 5.1). We then assess the need for an accurate model of the linear theory power spectrum and the relative merits of the general and parametric fitting procedures (Section 5.2). In Section 5.3, we present our main results, which are summarized in Fig. 19 and Table 2, which lists the best-fitting value of α and the estimated error for different samples of galaxies at $z = 1$, along with the corresponding fractional error in w. Finally, in Section 5.4, we use the results presented in Section 5.3 to make forecasts for the accuracy with which several forthcoming surveys will be able to measure the value of w.

5.1 The algorithm to extract the scale of the acoustic oscillations in action

We present a series of plots for samples at $z = 0$, which illustrate the various stages in the fitting process. Fig. 13 shows the power spectra measured for different tracers, both in real and redshift space. The sample of dark matter haloes includes all objects with a mass in excess of $5.4 \times 10^{12}\,h^{-1}\,{\rm M}_\odot$. The galaxy sample is magnitude limited with a space density of $\bar{n} = 5 \times 10^{-4}\,h^{-3}\,{\rm Mpc}^3$. For reference, the linear perturbation theory power spectrum for the mass at $z = 0$ is shown by the blue line in each panel: this is the power spectrum of the dark matter measured in real space at $z = 15$, scaled by the ratio of growth factors in order to have the amplitude expected at $z = 0$. It is important to bear in mind that the y-axis in this plot covers more

Table 2. The results of applying the general fitting procedure described in Section 4 to power spectra measured for different galaxy catalogues at $z = 0$ (top) and $z = 1$ (bottom). In each table, the first row gives the results for the dark matter and the final row lists results for a sample of dark matter haloes (all haloes with mass in excess of $2.7 \times 10^{13}\, h^{-1}\, \mathrm{M}_{\odot}$). The first column gives the label of the sample, as defined in Section 2. The second column gives the space density of galaxies. The first two samples, A and B, are constructed by applying a magnitude limit. Samples C–F are derived from sample A by applying a second selection criterion, as listed in the third column. Samples C and E correspond to the red and blue halves of sample A, respectively. Samples D and F comprise the 50 per cent of galaxies from sample A with the strongest and weakest (in terms of equivalent width) O II[3727] emission lines, respectively. Column 4 (10) gives the effective bias of the sample, computed from the square root of the ratio of the measured galaxy power spectrum in real (redshift) space to the real-space power spectrum of the dark matter over the wavenumber interval $0.01 < k\,(h\,\mathrm{Mpc}^{-1}) < 0.05$. Column 5 (11) gives the ratio of the clustering signal to the shot noise for the power-spectrum measurement, averaged over the wavenumber range $0.19 < k\,(h\,\mathrm{Mpc}^{-1}) < 0.21$. Columns 6 and 7 (12 and 13) give the best-fitting values of the scaling parameter α and the 1σ error on the fit, in real (redshift) space. Column 9 (15) gives the error expected on the scale parameter from Seo & Eisenstein (2007). The rms Lagrangian displacement was set equal to 1 over the best-fitting non-linear scale ($1/k_{\mathrm{nl}}$) for each case.

ID	Sel I $\bar{n}$ (h^3 Mpc^{-3})	Sel II	Real space b	$\bar{n}P$	k_{nl} (h Mpc^{-1})	α	$\Delta\alpha$ (per cent)	$\Delta\alpha$ (per cent) (SE07)	Redshift space b	$\bar{n}P$	k_{nl} (h Mpc^{-1})	α	$\Delta\alpha$ (per cent)	$\Delta\alpha$ (per cent) (SE07)
						$z = 0$								
DM			0.99	3567	0.120	0.993	0.91	1.02	1.15	3635	0.110	0.989	1.05	1.17
A	5.0e−4		1.18	1.78	0.144	0.975	1.16	1.10	1.32	2.15	0.125	0.972	1.26	1.23
B	2.5e−4		1.33	1.11	0.155	0.971	1.34	1.18	1.47	1.34	0.139	0.966	1.35	1.23
C	2.5e−4	Red	1.32	1.15	0.152	0.978	1.35	1.21	1.46	1.36	0.127	0.975	1.49	1.37
D	2.5e−4	Strong	1.06	0.67	0.155	0.956	1.75	1.41	1.20	0.86	0.138	0.956	1.67	1.42
E	2.5e−4	Blue	1.03	0.66	0.141	0.964	1.92	1.56	1.17	0.83	0.130	0.962	1.79	1.53
F	2.5e−4	Weak	1.30	1.16	0.132	0.980	1.55	1.40	1.44	1.34	0.115	0.972	1.66	1.54
Haloes	5.9e−5		1.56	0.81	0.197	0.980	1.32	1.07	1.71	1.04	0.148	0.975	1.43	1.25
						$z = 1$								
DM			0.99	1269	0.163	0.997	0.61	0.68	1.29	1710	0.133	0.991	0.77	0.88
A	5.0e−4		1.34	0.87	0.188	0.980	1.30	1.10	1.60	1.19	0.164	0.976	1.21	1.07
B	2.5e−4		1.31	0.43	0.212	0.975	2.02	1.47	1.57	0.59	0.174	0.970	1.72	1.38
C	2.5e−4	Red	1.39	0.48	0.235	0.977	1.81	1.32	1.65	0.65	0.208	0.975	1.52	1.17
D	2.5e−4	Strong	1.31	0.40	0.624	0.971	1.90	1.14	1.57	0.55	0.186	0.970	1.79	1.31
E	2.5e−4	Blue	1.30	0.40	0.219	0.973	2.31	1.47	1.56	0.54	0.159	0.962	1.98	1.48
F	2.5e−4	Weak	1.37	0.47	0.218	0.987	1.91	1.38	1.63	0.64	0.190	0.978	1.61	1.25
Haloes	5.9e−5		3.07	0.59	0.226	1.000	1.65	1.24	3.34	0.77	0.146	0.994	1.82	1.53

than a factor of 1000 in amplitude. Fig. 13 shows that there is considerable variation in the power spectra measured for different types of objects, and between the results in real and redshift space, which reinforces the points made in Section 3 regarding deviations from the predictions of linear perturbation theory on large scales. The red curve in each panel shows the corresponding reference power spectrum, which is constructed from the measured power spectrum as explained in Section 4.

In Fig. 14, the symbols show the ratio obtained by dividing the measured power spectrum by the appropriate reference spectrum for the same samples plotted in Fig. 13. The ratios look remarkably similar for the different tracers up to $k \approx 0.15\, h\,\mathrm{Mpc}^{-1}$. Beyond this wavenumber, the appearance of the oscillations varies from panel to panel, but the ratio stays close to unity. This similarity illustrates how well the approach for producing the reference spectrum works. The red curves in each panel show the best-fitting model produced in the general scheme whilst the blue curves show the fit obtained in the parametric approach. The best fits have somewhat different forms at wavenumbers below $k \sim 0.05\, h\,\mathrm{Mpc}^{-1}$. The constraints on the values of the parameters k_{nl} and α are presented in Fig. 15, where we show the 1, 2 and 3σ ranges in the case of two parameters, computed assuming Gaussian errors. There is a weak systematic trend for the best-fitting result for α to shift to lower values when galaxies are considered instead of the dark matter. The errors on the recovered parameters are larger in the case of galaxies than for the dark matter or for haloes, reflecting the lower signal-to-noise ratio of the predicted galaxy power spectrum.

5.2 Two tests of the algorithm

Before presenting the main results of applying our algorithm to extract the acoustic oscillation scales for various samples drawn from the BASICC run, we use the L-BASICC ensemble to address two questions. (1) How accurately do we need to model the linear perturbation theory matter power spectrum to avoid introducing a systematic bias into the results for the oscillation scale? (2) How does the performance of the new method for constraining the oscillation scale introduced in this paper compare with earlier approaches? To help answer these questions, we use the power spectrum of the dark matter measured from the L-BASICC runs in real space at $z = 0$ and 3.8, the highest output redshift besides the initial conditions. The results of applying our standard algorithm for extracting the oscillation scale are shown by the red histogram labelled CAMB in Fig. 16, which gives the distribution of the best-fitting value of α. The ensemble returns an unbiased mean value for the stretch parameter, $\alpha = 1$. At $z = 3.8$, the standard deviation on the best fit is 0.3 per cent; by $z = 0$, this rises to 1 per cent.

To address the first issue above, regarding how well we need to model the linear theory power spectrum to get an unbiased result for the oscillation scale, we replace the CAMB generated power spectrum in our algorithm by the approximation introduced by Eisenstein & Hu (1998). These authors proposed a physically motivated expression for the linear theory power spectrum, with parameters set to achieve a reasonable match to the results obtained from detailed calculations using Boltzmann codes over a much wider range of

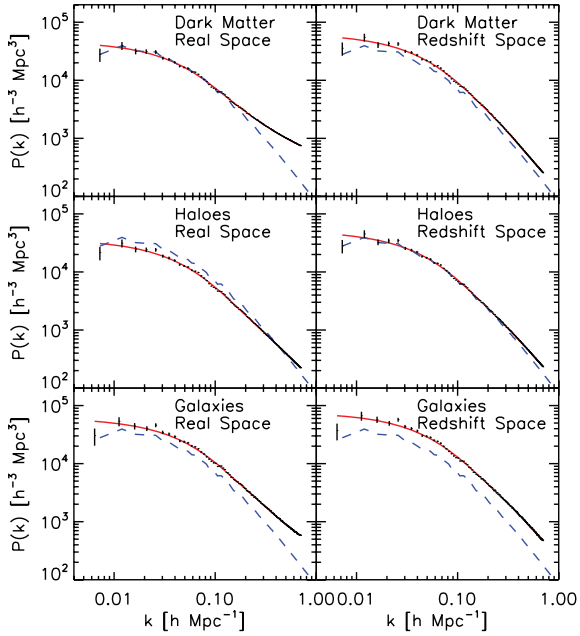

Figure 13. The power spectra of dark matter particles, dark matter haloes and galaxies at $z = 0$ (error bars). The real-space power spectra are plotted in the left-hand column and the redshift-space power spectra appear in the right-hand column. The red curves show the reference spectra derived from the measured spectra using a cubic spline fit, as described in Section 4. The blue curve is the same in each panel, showing the linear perturbation theory prediction for the $z = 0$ matter power spectrum (plotted using a high-redshift output obtained from the BASICC simulation, which has been scaled in amplitude according to the difference in growth factors between the two epochs expected in linear perturbation theory) The errors on the power spectrum are estimated using equation (3).

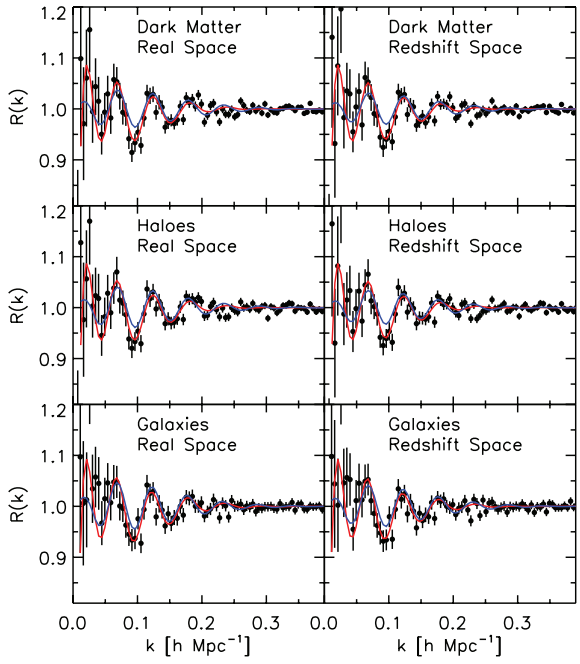

Figure 14. The ratio of the measured power spectrum divided by a smooth reference spectrum. The symbols correspond to the measurements plotted in Fig. 13 divided by the red curve in each panel of that figure. The red lines here show the best-fitting model in each case using the general method and the blue curves show the best fit for the parametric method. The errors on the power spectrum are estimated using equation (3).

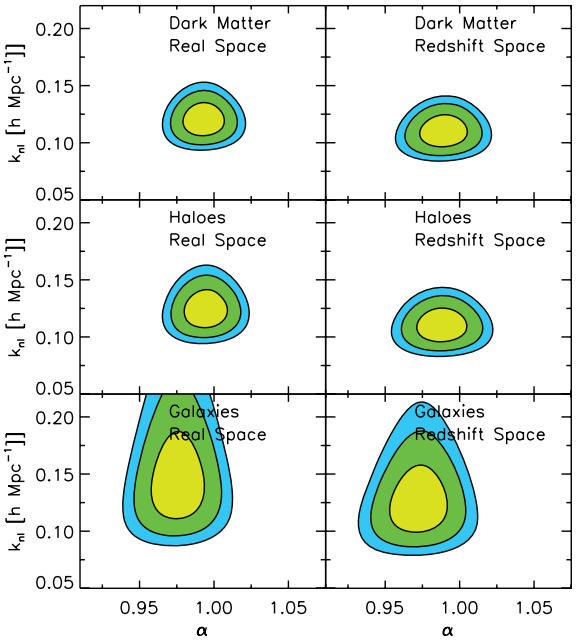

Figure 15. The constraints on the parameters $k_{\rm nl}$ and α for the power spectra plotted in Fig. 13. The contours show the 1, 2 and 3σ confidence limits for two parameters.

wavenumbers than are typically considered for BAO. Eisenstein & Hu's motivation was to provide physical insight into the form of the power spectrum in a CDM universe and to produce a code which could rapidly calculate large numbers of power spectra for grids cosmological parameters. Of course, the correct approach in our fitting procedure is to use the same code to compute the linear theory spectrum as was used to generate the initial conditions in the N-body simulation. In the case of real data, we do not have the luxury of knowing which Boltzmann code to use, so we should use the one which claims to be the most accurate representation of the model we are testing. Nevertheless, it is instructive to perform this test to see what error is introduced by using a less accurate calculation of the transfer function. The choice of Eisenstein & Hu's code is particularly relevant for this purpose as Blake & Glazebrook used this formalism to inspire their parametric expression to fit the acoustic oscillations. The use of Eisenstein & Hu's formalism to model the linear theory power spectra generated with CAMB introduces a small but measurable systematic shift in the mean value of α. At $z = 0$, the mean α indicated by the blue histogram in Fig. 16 is 0.98 ± 0.01.

We answer the second question by adopting the fitting algorithm of Blake & Glazebrook (2003), which assumes a parametric form for the ratio of the power spectrum with baryons to a smooth, CDM-only power spectrum. Changing the fitting method in this way also introduces a similar magnitude of shift in the best-fitting value of α. The green histogram shows the results when we use the parametric approach introduced by Blake & Glazebrook (2003). The mean value of α in this case is 1.01 ± 0.01. These shifts are small but one must bear in mind that the corresponding bias in the dark energy equation of state parameter is several times larger than the shift in α.

5.3 The main results

We now turn our attention back to the general results shown in Figs 17 and 18, and discuss the conclusions for different tracers

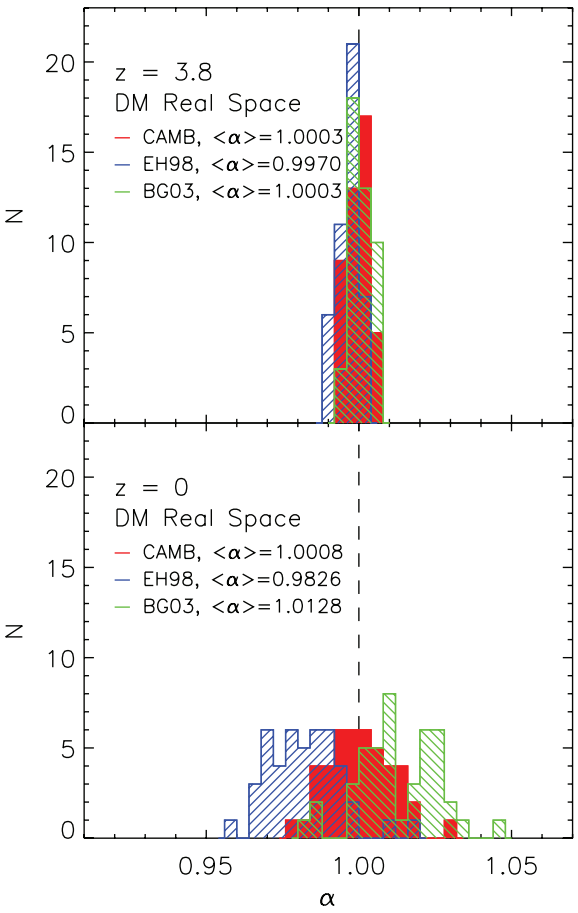

Figure 16. The best-fitting value for the scaling parameter α, recovered from the ensemble of low-resolution simulations, using the dark matter power spectrum in real space. The results are show for two different redshifts: $z = 3.8$ (top) and $z = 0$ (bottom). The histograms marked CAMB and BG03 show the results for the general and parametric fitting procedures, respectively. The blue histogram shows the results if the general method is followed with the CAMB power spectrum replaced by the formula for the linear theory power spectrum presented by Eisenstein & Hu (1998).

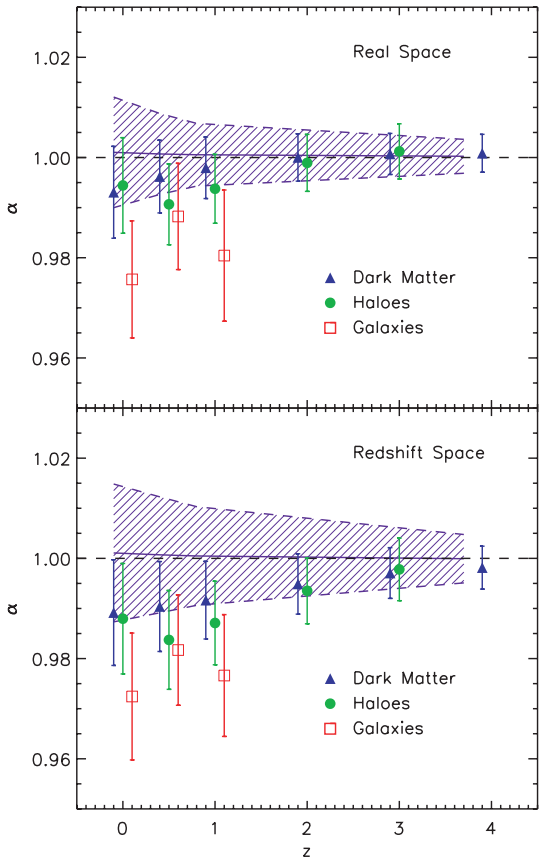

Figure 17. The best-fitting value of the scalefactor α as a function of redshift, for different tracers of the density distribution, in real space (top) and redshift space (bottom). The symbols show results from the high-resolution BASICC simulation: dark matter (blue triangles), dark matter haloes with mass in excess of $5.4 \times 10^{12}\,h^{-1}\,\mathrm{M}_{\odot}$ (green circles) and galaxies (red squares). The error bars show the 1σ range on α, calculated from $\Delta\chi^2$. The hatched region shows the central 68 per cent range of the results obtained using the dark matter in the ensemble of low-resolution simulations. Recall that $\alpha = 1$ corresponds to an unbiased measurement of the equation of state parameter, w, and that $\delta w \approx 4\delta\alpha$ at $z = 1$.

of the density field in turn. In these plots, the symbols refer to the constraints obtained from the high-resolution BASICC simulation and the shading shows results from the ensemble of low-resolution simulations, L-BASICC.

The blue triangles in Fig. 17 show the values obtained for α from the power spectrum of the dark matter. There is a trend for the best-fitting value to deviate away from unity with decreasing redshift, although the result at $z = 0$ is still within 1σ of $\alpha = 1$. The mean of the ensemble of low-resolution runs does not, however, show any deviation away from $\alpha = 1$ as a function of redshift, although the scatter on the recovered value of α increases towards the present day. If we examine the analogous results for individual simulations taken from the low-resolution ensemble, we find a wide range of behaviour for the best-fitting value of α for the dark matter. Some low-resolution runs give results which look like the high-resolution one, whereas others show deviations away from $\alpha = 1$, with values of $\alpha > 1$, as $z = 0$ is approached. The trend seen for the dark matter in the high-resolution run serves to illustrate the importance of sampling fluctuations, even in such large volumes. In redshift space, the scatter in the recovered value of α is larger than in real space (see also Seo & Eisenstein 2005; Eisenstein et al. 2007).

To obtain the errors quoted in Table 2 on the parameters α and $k_{\rm nl}$, we assume Gaussian mode counting errors on the power spectra measured in the BASICC simulation, as given by equation (3). In Fig. 3, we showed that this simple estimate of the errors on the power spectrum agreed fairly well with the scatter found in the measurements from the L-BASICC ensemble, particularly for the case of the dark matter. We have extended this comparison to look at how the errors on α and $k_{\rm nl}$ quoted in Table 2 match the scatter in these parameters obtained from the L-BASICC runs. We find the scatter estimated from the ensemble is somewhat larger than the error inferred using the mode counting argument. At $z = 0$, the mode counting errors are 20 per cent smaller for α for the dark matter in real space. In redshift space, the discrepancy increases to nearly 30 per cent. The mismatch between the two estimates is smaller at $z = 1$. The level of disagreement is not remarkable. It could be the case that the scatter from the ensemble has not converged, even with 50 realizations of the density field. A more likely explanation, particularly in view of the redshift dependence of the discrepancy, is mode coupling in the power-spectrum measurements arising from non-linearities and redshift-space distortions, which could increase

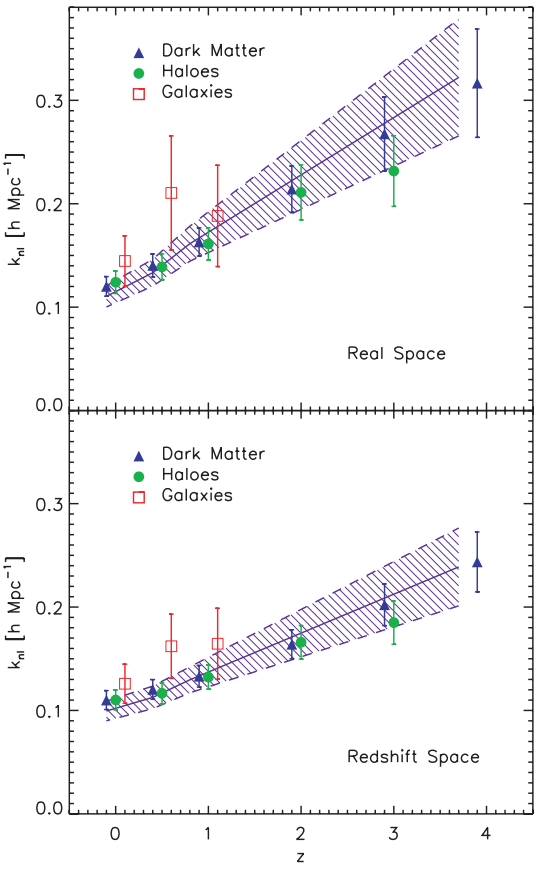

Figure 18. The best-fitting value of the damping scale $k_{\rm nl}$ as a function of redshift, for different tracers of the density distribution, in real space (top) and redshift space (bottom). The symbols show results from the high-resolution BASICC simulation: dark matter (blue triangles), dark matter haloes with mass in excess of $5.4 \times 10^{12}\,h^{-1}\,{\rm M}_{\odot}$ (green circles) and galaxies (red squares). The error bars show the 1σ range on α. The hatched region shows the central 68 per cent range of the results obtained using the dark matter in the ensemble of low-resolution simulations.

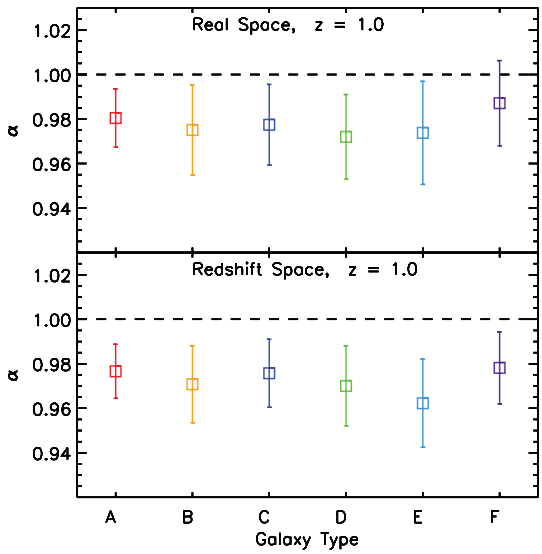

Figure 19. The recovered value of the stretch parameter α for the galaxy samples listed in Table 2. Recall that $\alpha = 1$ corresponds to the equation of state parameter $w = -1$. At $z = 1$, a shift in α away from unity implies a shift in the recovered value of w given by $\delta w \approx 4\delta\alpha$.

the variance in the power spectrum compared with the Gaussian estimate.

Fig. 18 shows that there is a strong trend for the best-fitting value of the smoothing scale, $k_{\rm nl}$, to decrease with decreasing redshift. This results from the oscillations being erased and modified down to smaller wavenumbers as the non-linearities in the density field grow. The variation of the smoothing scale $k_{\rm nl}$ on redshift is well described by a linear relation: $k_{\rm nl} = a + bz$. In real space, $a = 0.108 \pm 0.0082$ and $b = 0.054 \pm 0.0110$. In redshift space, $a = 0.096 \pm 0.0074$ and $b = 0.036 \pm 0.0094$.

The constraints on α and $k_{\rm nl}$ for dark matter haloes (with masses in excess of $5 \times 10^{12}\,h^{-1}\,{\rm M}_{\odot}$) are plotted with green circles in Figs 17 and 18. The parameter constraints obtained for this sample of haloes are very similar to those found for the dark matter, except for the value of $k_{\rm nl}$ at high redshift. Considering haloes in place of dark matter represents a step closer to the observations, so it is reassuring that the conclusions do not change significantly.

Finally, in Figs 17 and 18, we show using red squares the results for magnitude-limited samples of galaxies. The magnitude limit is varied with redshift such that in each case the galaxy sample has a space density $\bar{n} = 5 \times 10^{-4}\,h^{-3}\,{\rm Mpc}^3$. There is a weak systematic shift in the best-fitting values of α compared with the results obtained for the dark matter. At the same time the signal-to-noise ratio of the power-spectrum measurement is lower for the galaxy samples than for the dark matter, so the errors on the best-fitting parameters are correspondingly larger for the galaxies. The galaxy samples are consistent with $\alpha = 1$ at slightly over 1σ. The size of this systematic shift is comparable to the random measurement errors, so we cannot reach a firm conclusion. It will be very interesting to repeat our calculation with a larger simulation volume to reduce the size of the random errors and to assess if such shifts could genuinely provide an ultimate limitation to the accuracy of this method.

As a result of using a semi-analytic galaxy formation model which makes predictions for the observable properties of galaxies, we can vary the selection criteria used to construct samples and compare the constraints on the equation of state. The results of this exercise at $z = 1$ are presented in Table 2 and in Fig. 19, where we consider a range of samples defined either by a simple magnitude limit, or by a magnitude limit applied in combination with a colour cut or a restriction on the strength of an emission line. The key result from comparing the constraints for different samples is that whilst there are no strong systematic differences between the results, the accuracy of the constraints varies significantly. For example, using a catalogue of red galaxies, we predict that one could measure the dark energy equation of state with an accuracy 40 per cent better than that with the same number density of galaxies chosen by the strength of their emission lines.

We compare the error on the acoustic scale extracted from our simulations with the results of the prescription set out by Seo & Eisenstein (2007). The Seo & Eisenstein (2007) algorithm contains a parameter which is equivalent to $1/k_{\rm nl}$. If we use our best-fitting values of $k_{\rm nl}$, we find that the Seo & Eisenstein prescription gives a similar estimate of the error on the acoustic scale to that we obtain by fitting directly to the simulation results. However, if we use the value of $k_{\rm nl}$ suggested by Seo & Eisenstein (2007), which they extract from a dark matter simulation, we find that their prescription gives an optimistic estimate of the error on α. The reason we recover a larger value of $k_{\rm nl}$ from our galaxy samples than we do for the dark matter is due to the increased discreteness shot noise in these

samples, which results in noisier power spectra at high k. This causes an elongation in the confidence levels in the $k_{\rm nl}$ versus α plane.

It is interesting to compare the results for the dark matter and for the galaxy samples with those for a set of massive haloes. Table 2 also gives the constraints on α and $k_{\rm nl}$ for a sample of massive haloes (see also Angulo et al. 2005). There are 142 000 haloes in the BASICC output at z=1 with a mass in excess of $2.7 \times 10^{13}\, h^{-1}\, {\rm M}_{\odot}$. Although the effective bias of this sample of massive haloes is greater than that of any of the galaxy samples listed in Table 2, the reduction in space density means that $\bar{n}P \approx 1$ and the estimated error on w is comparable to that found for the galaxy samples.

5.4 Forecasts for future surveys

We can use the results presented in Table 2 to make a rough estimate of the accuracy with which future surveys are likely to be able to constrain the scale of the acoustic oscillations. This can be done using a simple calculation motivated by the expression for the fractional error in the power spectrum given by equation (3). We assume that the error in the distance scale, $\Delta\alpha$, scales with the volume of the survey, $V_{\rm survey}$, and the product of the space density of galaxies and the power spectrum, $\bar{n}P(k = 0.2\, h\, {\rm Mpc}^{-1})$, as

$$\Delta\alpha \propto \frac{1}{\sqrt{V_{\rm survey}}} \left(1 + \frac{1}{\bar{n}P}\right). \quad (15)$$

The constant of proportionality can be set for a particular galaxy sample using the results given in Table 2.

The WiggleZ survey is currently underway and will measure redshifts for 400 000 blue galaxies over 1000 deg^2 in the redshift interval $z = 0.5$–1.0 (Glazebrook et al. 2007). For the cosmological parameters adopted in this paper, this gives a comoving volume of $1.13\, h^{-3}\, {\rm Gpc}^3$. Using the blue colour selected sample or the large equivalent width sample from Table 2, and assuming $\bar{n}P \sim 1$ for WiggleZ galaxies, somewhat higher than we find in our simulation, we estimate that this survey will measure the distance scale to an accuracy of $\Delta\alpha \sim 2$ per cent, which is similar to that claimed by Glazebrook et al. using linear perturbation theory.

The WFMOS survey has been proposed to motivate the construction of a new spectrograph for the Subaru telescope (Glazebrook et al. 2005). This will target galaxies with a space density of $\bar{n} = 5 \times 10^{-4}\, h^3\, {\rm Mpc}^{-3}$ in the redshift interval $z = 0.5$–1.3 over 2000 deg^2, covering a volume of $4.4\, h^{-3}\, {\rm Gpc}^3$. (There is also a WFMOS survey which will target $z = 3$ galaxies but over a much smaller solid angle.) Using sample A from Table 2, and adopting $\bar{n}P = 1$, we obtain an estimated error of $\Delta\alpha = 0.83$ per cent, again in good agreement with Glazebrook et al.

Photometric surveys can generally cover a larger solid angle than spectroscopic surveys down to a fainter magnitude limit. The fainter magnitude limit results in a higher median redshift and a broader redshift distribution for the survey galaxies, which means that a larger volume is covered. However, the limited accuracy of photometric redshift estimates means that in practice Fourier modes are lost and the effective volume of the survey is greatly reduced. Blake & Bridle (2005) estimate that the factor by which the survey volume is reduced is $\approx 12(\delta z/(1+z)/0.03)$, where $\delta z/(1+z)$ is the error in the photometric redshifts.

The Panoramic Survey Telescope and Rapid Response System (Pan-STARRS) survey will map 3π sr of the sky (http://pan-starrs.ifa.hawaii.edu/public/home.html). Cai et al. (in preparation) show that the median redshift of the 3π survey will be $z \approx 0.5$, with a tail extending to $z \approx 1.2$. The volume of the survey, assuming that 20 000 deg^2 cover low-extinction parts of the sky and give high-quality clustering measurements, is around $41\, h^{-3}\, {\rm Gpc}^3$. Talking sample A from Table 2, and setting $\bar{n}P \gg 1$, as appropriate for the relatively high space density of galaxies in a photometric sample, and allowing for the reduction in the effective volume caused by a photometric redshift error of $\delta z/(1+z) = 0.03$, gives a forecast error on the oscillation scale of $\Delta\alpha \sim 0.5$ per cent. In the more likely event that the photometric redshift errors are twice as large, $\delta z/(1+z) \sim 0.06$, this figure increases to $\Delta\alpha \sim 0.7$ per cent.

Remembering the crude conversion $\Delta w \approx 4\, \Delta\alpha$ from Section 4, this means that the next generation of galaxy surveys is unlikely to deliver 1 per cent errors on a constant equation of state from BAO measurements used in isolation from other cosmological data. A survey with almost an order of magnitude more effective volume than Pan-STARRS will be needed to achieve this target. This will require an all-sky, spectroscopic galaxy redshift survey, such as the SPACE mission being proposed to ESA's Cosmic Vision call. SPACE will measure redshifts for galaxies in the interval $0.5 < z < 2$, covering around $150\, h^{-3}\, {\rm Gpc}^3$. Extrapolating from Sample A, we forecast that an error in the oscillation scale of $\Delta\alpha \sim 0.15$ per cent could be achieved with SPACE. In the case of the pessimistic translation to an error on w considered in Section 4, this corresponds to $\Delta w \sim 0.6$ per cent; in the optimistic scenario, we expect a constraint of $\Delta w \sim 0.23$ per cent.

6 CONCLUSIONS

In the next 5–10 yr, several proposed galaxy surveys will allow high-precision measurements of the clustering of galaxies on the scale of the acoustic oscillations at intermediate and high redshifts. Both photometric and spectroscopic surveys are planned, which will cover volumes up to tens of cubic gigaparsecs and will contain hundreds of thousands to hundreds of millions of galaxies. There is a clear need to ensure that theoretical predictions develop apace with sufficient accuracy and realism to allow such data sets to be fully exploited and to uncover any possible systematic errors in this cosmological test to uncover the nature of the dark energy.

Early theoretical work in this area used linear perturbation theory (Blake & Glazebrook 2003; Hu & Haiman 2003; Glazebrook & Blake 2005). Recently, more physical calculations have been carried out using N-body simulations with cubes of side 500–1100 h^{-1} Mpc (Seo & Eisenstein 2003, 2005; Schulz & White 2006; Huff et al. 2007; Seo & Eisenstein 2007). In this paper, we have improved upon previous modelling work in three ways. First, we have used a simulation volume comparable to the largest of the currently proposed spectroscopic surveys. This allows us to accurately follow the growth of density fluctuations on an ultralarge scales in excess $100\, h^{-1}$ Mpc, the scales of interest for the acoustic oscillations, which can only be followed approximately in smaller computational volumes. In particular, a large volume is necessary to obtain accurate predictions for bulk flows, which are sensitive to the power spectrum at low wavenumbers. The only published work with a larger simulation volume used the Hubble Volume Simulation (Angulo et al. 2005; Koehler et al. 2007). The Hubble Volume has a larger particle mass than the BASICC, which restricted these studies to consider either cluster mass dark matter haloes (Angulo et al. 2005) or a simple biasing scheme to add galaxies (Koehler et al. 2007). Secondly, through the use of a large number of particles, we are able to resolve the majority of the haloes which are likely to host the galaxies which will be observed in the forthcoming surveys. Thirdly, we use a semi-analytic galaxy formation model to populate the simulation with galaxies. Unlike other studies which use phenomenological biasing schemes or the halo occupation model to add galaxies, this

allows us to predict the shape and amplitude of the galaxy power spectrum and the signal-to-noise ratio of the clustering expected for different galaxy selections.

We use our *N*-body simulation in combination with a galaxy formation model to make the connection between the linear perturbation theory prediction for the matter power spectrum and the power spectrum of galaxies. We do this in a series of steps, starting with power spectrum of the dark matter, looking at the impact of the non-linear growth of fluctuations and peculiar motions or redshift-space distortions, before examining the power spectrum of dark matter haloes and, finally, galaxies. A number of conclusions are reached from this study. (i) The non-linear evolution of the dark matter power spectrum is apparent even on scales larger than the sound horizon scale. Although the deviation from linear theory is only a few per cent, the coupled evolution of different Fourier modes means that these scales need to be followed accurately to get the correct behaviour at higher wavenumbers. (ii) The form of the distortion of the power spectrum due to peculiar motions is extremely sensitive to the type of object under consideration, being quite different for the cases of dark matter, dark haloes and galaxies. Moreover, different galaxy selections give different redshift-space distortions. (iii) Galaxy bias is scale dependent and sensitive to the selection applied for wavenumbers $k > 0.15\,h\,\mathrm{Mpc}^{-1}$. Eisenstein et al. (2007) discuss a technique which attempts to reconstruct the linear density field from an observed distribution of objects. The reconstruction can reduce the damping of the higher harmonic oscillations in the power spectrum, thereby increasing the statistical significance of the acoustic scale measurement and diminishing any systematic effects caused by departures from linearity. It will be interesting to apply this method to the galaxy samples presented in this paper, to see if this approach still works at the required level in the case of biased tracers of the linear density field.

We also present a new method to extract the dark energy equation of state parameter, based upon an approach put forward by Percival et al. (2007). The method involves dividing the measured power spectrum by a smooth reference spectrum and comparing the resulting ratio to the predictions of linear perturbation theory. The algorithm has three key advances over earlier work, which can be credited to Eisenstein et al. (2005) and Percival et al. (2007). (i) The reference spectrum is derived from the measured spectrum, which avoids the need to apply major corrections to a linear theory reference. (ii) The measured ratio is compared to a prediction generated using CAMB, which is more accurate than assuming a parametric form for the ratio based on a Taylor expansion. (iii) The linear theory ratio is modified by allowing the higher order oscillations to be damped, which improves the fit to the measured ratio. Changing the value of the equation of state parameter is approximately equivalent to rescaling the wavenumber in the predicted power-spectrum ratio; at $z = 1$, a 1 per cent shift in wavenumber is equivalent to a 4 per cent shift in the recovered value of w.

We explore the constraints on the dark energy equation of state using different tracers of the density field. By applying our algorithm for extracting the oscillation scale to the L-BASICC ensemble, we have provided the most stringent test to date of usefulness of BAO for measuring the equation of state of the dark energy. For the case of the dark matter, there is no significant bias in the recovered oscillation scale, compared with the value expected from linear perturbation theory. Within a given simulation, we find that 1 per cent deviations from the underlying length-scale are possible although these are only at the 1σ level. Such excursions are the result of sampling variance arising from the finite volume of the computational box, which are important even in a simulation of the volume of the BASICC. The error on the scalefactor recovered from galaxy samples is larger than that found for the dark matter, reflecting the lower signal-to-noise ratio of the galaxy power-spectrum measurements. Different galaxy selections lead to variations in the clustering strength and hence in the error expected in the scalefactor.

Currently, the best constraints on the equation of state parameter come either from combining data sets, such as the power spectrum of galaxy clustering and measurements of the microwave background radiation (e.g. Sánchez et al. 2006) or from the Hubble diagram of Type Ia, with priors on the flatness of the Universe and the matter density (Riess et al. 2004). For example, Wood-Vasey et al. (2007)combine high-redshift SNe Ia from the ESSENCE Supernova Survey with the measurement of the BAO made by Eisenstein et al. (2005), and, assuming a flat universe, constrain a constant equation of state to have $w = -1.05^{+0.13}_{-0.12}(\mathrm{statistical}) \pm 0.11(\mathrm{systematic})$, consistent with a cosmological constant. Possible contributions to the systematic error include the degree of dust extinction in the SNe host galaxy, evolution in the properties of SNe with redshift and local calibration effects such as a 'Hubble bubble'. We have used our simulation results to forecast the accuracy with which future galaxy surveys will use the BAO in isolation to constrain the scale of the acoustic oscillations, and under certain assumptions, w. We anticipate that Pan-STARRS, with accurate photometric redshifts, will have an accuracy comparable to that expected for the next generation of spectroscopic survey (WFMOS) and could potentially reduce the statistical errors on the value of w by a factor of 2 compared with the current constraints. However, the target of 1 per cent random errors on w using BAO measurements is beyond the grasp of any of the surveys likely to be completed or even to start within the next decade.

The predictions we have presented here are idealized in a number of respects. The accuracy with which we expect the dark energy equation of state parameter will be measured assumes that the values of the other cosmological parameters are known with infinite accuracy. We have also neglected the impact of the survey window function on the power-spectrum measurement; this will be particularly important in the case of surveys which rely on photometric redshifts. In future work, we plan a number of improvements. (i) Use of an even larger simulation volume, to exceed that proposed in forthcoming surveys. One caveat on our quoted error on w is that some of the planned surveys will be larger than the volume of the BASICC, and will consequently have smaller sampling fluctuations. (ii) The inclusion of the evolution of clustering along the line of sight. Although we have focused on $z = 1$, proposed surveys will span a broad redshift interval centred on this value. (iii) The inclusion of a survey window function, mimicking the angular and radial selections, and including the impact of errors on photometric redshifts. Such calculations represent huge challenges in computational cosmology, due to the volume coverage and mass resolution required in the *N*-body simulations used, and the post-processing needed to include galaxies. However, such calculations are essential if the BAO approach is to be used to its full potential.

ACKNOWLEDGMENTS

We are indebted to Volker Springel for providing us with a stripped down version of his GADGET-2 code and to the Virgo Consortium for access to their supercomputing resources. Lydia Heck provided vital system management support which made this project feasible. We thank the referee, Daniel Eisenstein, for providing a thorough and helpful report. We acknowledge useful conversations and comments on the draft from Richard Bower, Shaun Cole, Martin Crocce,

Ariel Sanchez, Liang Gao, Adrian Jenkins, Volker Springel, Enrique Gaztanaga, Francisco Castander, Pablo Fosalba and Will Sutherland. This work was supported in part by the Particle Physics and Astronomy Research Council, the European Commission through the ALFA-II programme's funding of the Latin-American European Network for Astrophysics and Cosmology (LENAC), and the Royal Society, through the award of a Joint Project grant and its support of CMB.

REFERENCES

Albrecht A. et al., 2006, preprint (astro-ph/0609591)
Alcock C., Paczynski B., 1979, Nat, 281, 358
Almeida C., Baugh C. M., Lacey C. G., 2007a, MNRAS, 376, 1711
Almeida C., Baugh C. M., Wake D. A., Lacey C. G., Bensen A. J., Bower R. G., Pimbblet K., 2007b, MNRAS, submitted (arXiv:0710.3557)
Angulo R., Baugh C. M., Frenk C. S., Bower R. G., Jenkins A., Morris S. L., 2005, MNRAS, 362, L25
Baugh C. M., 2006, Rep. Prog. Phys., 69, 3101
Baugh C. M., Efstathiou G., 1994, MNRAS, 270, 183
Baugh C. M., Gaztanaga E., Efstathiou G., 1995, MNRAS, 274, 1049
Baugh C. M., Lacey C. G., Frenk C. S., Granato G. L., Silva L., Bressan A., Benson A. J., Cole S., 2005, MNRAS, 356, 1191
Benson A. J., Cole S., Frenk C. S., Baugh C. M., Lacey C. G., 2000, MNRAS, 311, 793
Benson A. J., Frenk C. S., Lacey C. G., Baugh C. M., Cole S., 2002, MNRAS, 333, 177
Benson A. J., Bower R. G., Frenk C. S., Lacey C. G., Baugh C. M., Cole S., 2003, ApJ, 599, 38
Berlind A. A. et al., 2003, ApJ, 593, 1
Bertschinger B., 1998, ARA&A, 36, 599
Blake C., Bridle S., 2005, MNRAS, 363, 1329
Blake C., Glazebrook K., 2003, ApJ, 594, 665
Blake C., Parkinson D., Bassett B., Glazebrook K., Kunz M., Nichol R. C., 2006, MNRAS, 365, 255
Blake C., Collister A., Bridle S., Lahav O., 2007, MNRAS, 374, 1527
Bower R. G., Benson A. J., Malbon R., Helly J. C., Frenk C. S., Baugh C. M., Cole S., Lacey C. G., 2006, MNRAS, 370, 645
Carroll S. M., Press W. H., Turner E. L., 1992, ARA&A, 30, 499
Colberg J. M. et al., 2000, MNRAS, 319, 209
Cole S., Kaiser N., 1989, MNRAS, 237, 1127
Cole S., Hatton S., Weinberg D. H., Frenk C. S., 1998, MNRAS, 300, 945
Cole S., Lacey C. G., Baugh C. M., Frenk C. S., 2000, MNRAS, 319, 168
Cole S. et al., 2005, MNRAS, 362, 505
Cooray A., Sheth R., 2002, Phys. Rep., 372, 1
Crocce M., Scoccimarro R., 2006a, Phys. Rev. D, 73, 063520
Crocce M., Scoccimarro R., 2006b, Phys. Rev. D, 73, 063519
Crocce M., Pueblas S., Scoccimarro R., 2006, MNRAS, 373, 369
Croton D. J., Gao L., White S. D. M., 2007, MNRAS, 374, 1303
Davis M., Efstathiou G., Frenk C. S., White S. D. M., 1985, ApJ, 292, 371
Efsthathiou G., 1988, in Lawrence A., ed., Lecture Notes in Phys. Vol. 297, Proc. Third IRAS Conf., Comets to Cosmology. Springer-Verlag, Heidelberg, p. 312
Efstathiou G., Davis M., White S. D. M., Frenk C. S., 1985, ApJS, 57, 241
Eisenstein D. J., Hu W., 1998, ApJ, 496, 605
Eisenstein D. J. et al., 2005, ApJ, 633, 560
Eisenstein D. J., Seo H.-j., White M., 2007, ApJ, 664, 660
Evrard A. E. et al., 2002, ApJ, 573, 7
Feldman H. A., Kaiser N., Peacock J. A., 1994, ApJ, 426, 23
Gao L., Springel V., White S. D. M., 2005, MNRAS, 363, L66
Glazebrook K. et al., 2005, preprint (astro-ph/0507457)
Glazebrook K. et al., 2007, in Metcalfe N., Shanks T., eds, ASP Conf. Ser. Vol. 379, Cosmic Frontiers. Astron. Soc. Pac., San Francisco, in press (astro-ph/0701876)
Glazebrook K., Blake C., 2005, ApJ, 631, 1
Governato F., Babul A., Quinn T., Tozzi P., Baugh C. M., Katz N., Lake G., 1999, MNRAS, 307, 949
Hamilton A. J. S., Kumar P., Lu E., Matthews A., 1991, ApJ, 374, L1
Harker G., Cole S., Helly J., Frenk C., Jenkins A., 2006, MNRAS, 367, 1039
Hatton S. J., 1999, PhD thesis, Univ. Durham
Heath D. J., 1977, MNRAS, 179, 351
Hockney R. W., Eastwood J. W., 1981, Computer Simulation Using Particles. McGraw-Hill, New York
Hu W., Haiman Z., 2003, Phys. Rev. D, 68, 063004
Hu W., Sugiyama N., 1996, ApJ, 471, 542
Huff E., Schulz A. E., White M., Schlegel D. J., Warren M. S., 2007, Astropart. Phys., 26, 351
Hütsi G., 2006a, A&A, 449, 891
Hütsi G., 2006b, A&A, 459, 375
Jain B., Bertschinger E., 1994, ApJ, 431, 495
Jing Y. P., 1998, ApJ, 503, L9+
Jing Y. P., 2005, ApJ, 620, 559
Kaiser N., 1984, ApJ, 284, L9
Kaiser N., 1987, MNRAS, 227, 1
Kauffmann G., Nusser A., Steinmetz M., 1997, MNRAS, 286, 795
Koehler R. S., Schuecker P., Gebhardt K., 2007, A&A, 462, 7
Le Delliou M., Lacey C., Baugh C. M., Guiderdoni B., Bacon R., Courtois H., Sousbie T., Morris S. L., 2005, MNRAS, 357, L11
Le Delliou M., Lacey C. G., Baugh C. M., Morris S. L., 2006, MNRAS, 365, 712
Lewis A., Challinor A., Lasenby A., 2000, ApJ, 538, 473
Linder E. V., 2005, Phys. Rev. D, 72, 043529
Linder E. V., Cahn R. N., 2007, preprint (astro-ph/0701317)
Meiksin A., White M., Peacock J. A., 1999, MNRAS, 304, 851
Mo H. J., White S. D. M., 1996, MNRAS, 282, 347
Mo H.-J., Jing Y. P., White S. D. M., 1997, MNRAS, 284, 189
Nagashima M., Lacey C. G., Baugh C. M., Frenk C. S., Cole S., 2005a, MNRAS, 358, 1247
Nagashima M., Lacey C. G., Okamoto T., Baugh C. M., Frenk C. S., Cole S., 2005b, MNRAS, 363, L31
Padilla N. D., Baugh C. M., 2002, MNRAS, 329, 431
Padmanabhan N. et al., 2007, MNRAS, 378, 852
Parkinson D., Blake C., Kunz M., Bassett B. A., Nichol R. C., Glazebrook K., 2007, MNRAS, 377, 185
Peacock J., Schneider P., 2006, The Messenger, 125, 48
Peacock J. A., Dodds S. J., 1994, MNRAS, 267, 1020
Peacock J. A., Dodds S. J., 1996, MNRAS, 280, L19
Peacock J. A., Smith R. E., 2000, MNRAS, 318, 1144
Peebles P. J. E., 1980, The Large-scale Structure of the Universe. Research supported by the National Science Foundation. Princeton Univ. Press, Princeton, NJ, p. 435
Peebles P. J. E., Yu J. T., 1970, ApJ, 162, 815
Percival W. J., Baugh C. M., Bland-Hawthorn J., Bridges T., Cannon E. A., 2001, MNRAS, 327, 1297
Percival W. J. et al., 2007, ApJ, 657, 51
Perlmutter S. et al., 1999, ApJ, 517, 565
Press W. H., Schechter P., 1974, ApJ, 187, 425
Press W. H., Vishniac E. T., 1980, ApJ, 236, 323
Riess A. G. et al., 1998, AJ, 116, 1009
Riess A. G. et al., 2004, ApJ, 607, 665
Sánchez A. G., Baugh C. M., Percival W. J., Peacock J. A., Padilla N. D., Cole S., Frenk C. S., Norberg P., 2006, MNRAS, 366, 189
Schulz A. E., White M., 2006, Astropart. Phys., 25, 172
Scoccimarro R., 2004, Phys. Rev. D, 70, 083007
Scoccimarro R., Sheth R. K., Hui L., Jain B., 2001, ApJ, 546, 20
Seljak U., 2000, MNRAS, 318, 203
Seljak U., Warren M. S., 2004, MNRAS, 355, 129
Seo H.-J., Eisenstein D. J., 2003, ApJ, 598, 720
Seo H.-J., Eisenstein D. J., 2005, ApJ, 633, 575
Seo H.-J., Eisenstein D. J., 2007, ApJ, 665, 14
Sheth R. K., Mo H. J., Tormen G., 2001, MNRAS, 323, 1
Smith R. E. et al., 2003, MNRAS, 341, 1311
Smith R. E., Scoccimarro R., Sheth R. K., 2007, Phys. Rev. D, 75, 063512
Spergel D. N. et al., 2007, ApJS, 170, 377
Springel V., 2005, MNRAS, 364, 1105

Springel V. et al., 2005, Nat, 435, 629
Springel V., Frenk C. S., White S. D. M., 2006, Nat, 440, 1137
Sunyaev R. A., Zeldovich Y. B., 1970, Ap&SS, 7, 3
Tegmark M. et al., 2006, Phys. Rev. D, 74, 123507
Wechsler R. H., Zentner A. R., Bullock J. S., Kravtsov A. V., Allgood B., 2006, ApJ, 652, 71
Wetzel A. R., Cohn J. D., White M., Holz D. E., Warren M. S., 2007, ApJ, 656, 139
White S. D. M., 1994, preprint (astro-ph/94100943)
Wood-Vasey W. M. et al., 2007, ApJ, 666, 964
Zel'donch Y.-B., 1970, A&A, 5, 84
Zheng Z. et al., 2005, ApJ, 633, 791

This paper has been typeset from a TEX/LATEX file prepared by the author.